

From Feedback-Free Star Clusters to Little Red Dots via Compaction

AVISHAI DEKEL,¹ DHRUBA DUTTA CHOWDHURY,¹ SHARON LAPINER,¹ ZHIYUAN YAO,¹ SHMUEL GILBAUM,¹ DANIEL CEVERINO,²
JOEL PRIMACK,³ RACHEL SOMERVILLE,⁴ AND ROMAIN TEYSSIER⁵

¹*Racah Institute of Physics, The Hebrew University, Jerusalem 91904, Israel*

²*Departamento de Física Teórica and CIAFF, Facultad de Ciencias, Universidad Autónoma de Madrid, Cantoblanco, 28099 Madrid, Spain*

³*Department of Physics and SCIPP, University of California, Santa Cruz, CA 96064, USA*

⁴*Center for Computational Astrophysics, Flatiron Institute, 162 5th Avenue, New York, NY 10010, USA*

⁵*Department of Astrophysical Sciences, Princeton University, 4 Ivy Lane, Princeton, NJ 08540, USA*

ABSTRACT

We address the origin of the Little Red Dots (LRDs) seen by JWST at cosmic morning ($z=4-8$) as compact stellar systems with over-massive black holes (BHs). We propose that LRDs form naturally after feedback-free starbursts (FFB) in thousands of star clusters and following wet compaction. Analytically, we show how the clusters enable efficient dry migration of stars and BHs to the galaxy center by two-body segregation and dynamical friction against the disk. The clusters merge to form compact central clusters as observed. Mutual tidal stripping does not qualitatively affect the analysis. The young, rotating clusters are natural sites for the formation of BH seeds via rapid core collapse. The migrating clusters carry the BH seeds, which merge into central super-massive BHs (SMBHs). Compactions are required to deepen the potential wells such that the SMBHs are retained after post-merger gravitational-wave recoils, locked to the galaxy centers. Using cosmological simulations at different epochs, with different codes and physical recipes, we evaluate the additional growth of LRD-matching compact central stellar systems by global compaction events. Adding to the dry growth by cluster mergers, the compactions can increase the escape velocities to retain the SMBHs. The LRDs appear at $z \sim 8$, after the formation of FFB clusters, and disappear after $z \sim 4$ when the stellar mass is above $10^9 M_{\odot}$ by growing post-compaction blue disks around the nuclear LRDs. The LRD abundance is expected to be $\sim 10^{-5} - 10^{-4} \text{ Mpc}^{-3}$, increasing from $z \sim 4$ to $z \sim 8$.

Keywords: Galaxies (594) – Galaxies (595) – Galaxies (600) – Galaxies (734)

1. INTRODUCTION

1.1. Little Red Dots

JWST observations reveal the existence of a distinct population of galaxies termed Little Red Dots (LRDs), detected at cosmic morning in the redshift range $z = 4 - 8$ (e.g., G. Barro et al. 2024a,b; J. F. W. Baggen et al. 2024; F. Pacucci 2024; F. Pacucci & R. Narayan 2024; C. M. Casey et al. 2024, 2025; J. E. Greene et al. 2025; H. B. Akins et al. 2025a,b,c; F. Pacucci & A. Loeb 2025; F. Pacucci et al. 2025; A. J. Taylor et al. 2025b,a). Their high abundance is roughly 1.5–2 dex below the total abundance of galaxies at the same UV magnitude (e.g., V. Kokorev et al. 2024; J. E. Greene et al. 2024; D. D. Kocevski et al. 2025). The LRDs are characterized by compact, mostly unresolved red optical sizes. They tend to show a so called “V-shaped” spectral energy distribution (SED), blue in the UV and red in optical light. They show

broad permitted lines, with a flat IR spectrum, no far-IR/sub-mm emission and weak near-to-mid IR emission, and some show Balmer breaks. Typically, no X-ray or radio waves are detected.

The two extreme interpretations of LRDs are that they are either dominated by black holes (BHs) or by stars (e.g., F. Pacucci 2024; F. Pacucci & R. Narayan 2024). The BH-dominated interpretation would require a very high ratio of BH-to-stellar mass compared to low redshifts and an explanation for the undetected X-rays. The stellar-dominated interpretation would require extremely high stellar densities, not seen in other galaxies.

A hybrid interpretation is plausible, where the LRDs consist of both compact stellar systems and over-massive black holes. The hybrid model is supported by the observational finding of B. L. Jones et al. (2025) that most of the galaxies with over-massive BHs are LRDs. They examined a sample of 70 broad-line Active Galactic Nuclei (AGN) identified at $z = 3 - 7$ using NIRSpect/G395M spectroscopy from the CEERS,

JADES, and RUBIES JWST surveys. As can be seen in their illuminating Fig. 6, they find that 43% of the sample are classified as LRDs, a fraction that increases with redshift. These LRDs with BHs tend to be of lower stellar masses than the non-LRD AGN, with the BH-to-stellar mass ratio 1-2 dex above the low-redshift AGN and increasing with redshift. They have BH masses in the range $10^{6.7} - 10^{8.7} M_{\odot}$, high BH-to-stellar mass ratios of 0.01–0.1, and estimated stellar masses of $10^8 - 10^9 M_{\odot}$.

Before addressing the detailed properties of LRDs, the main basic challenge addressed here is to explain the formation of compact stellar systems with over-massive black holes at cosmic morning, and their apparent disappearance at later times.

1.2. FFB clusters

A straightforward physical model predicts a high star-formation efficiency, at the level of 0.2–0.3 for the global ratio of stars to accreted gas, under the conditions of high density and moderate metallicity that are valid in massive galaxies at cosmic dawn (A. Dekel et al. 2023; Z. Li et al. 2024). It is due to feedback-free starbursts (FFB) in thousands of star clusters within each galaxy. This is as opposed to the a star formation efficiency lower than 0.1 at lower redshifts, where feedback from stars and from AGN is expected to suppress star formation. The FFB phase is expected to occur at $z > 8$, in dark-matter halos of mass $M_{\text{vir}} > 10^{10.5} M_{\odot}$, with the threshold mass dropping steeply as a function of redshift, $M_{\text{vir}} \propto (1+z)^{-6.2}$. The typical resultant galaxy is a rather compact rotating disk of half-mass radius ~ 300 pc, consisting of thousands of rotating star clusters of masses in the range $10^4 - 10^7 M_{\odot}$ and radii of order 10 pc. These galaxies are predicted to have low gas fraction ($f_{\text{gas}} \sim 0.01 - 0.1$), relatively low metallicity ($Z \sim 0.01 - 0.1 Z_{\odot}$), and low dust attenuation ($A_{\text{UV}} \sim 0.5$). We propose that the FFB clusters serve as a key element in the formation of LRDs, both in the origin of a compact stellar system and in the growth of an over-massive central black hole.

The first cosmological simulation of a galaxy at cosmic dawn that is marginally capable of capturing the FFB main physical processes in clusters (Chen et al., in preparation) indeed reveals the formation of thousands of clusters. This is a simulation utilizing the GIZMO code (P. F. Hopkins 2015), with ≤ 3 pc gas resolution, which incorporates a 3.4 Myr delay in supernova feedback. The simulated cluster properties are found to largely resemble the FFB model predictions, including total mass, mass function, high densities, bursty star-formation history, high star-formation efficiency, low gas fraction, low metallicity, weak dust obscuration, and the migration of the massive clusters towards the galaxy center.

Cluster-dominated galaxies are indeed observed at cosmic morning. JWST observations using gravitational lensing re-

veal galaxies in the redshift range $z = 4 - 10$ in which the stellar mass is dominated by young massive star clusters (A. Claeysens et al. 2023; E. Vanzella et al. 2023; S. Fujimoto et al. 2023; M. Messa et al. 2024; A. Adamo et al. 2024; L. Mowla 2024; L. Mowla et al. 2024). They are descriptively dubbed “Sunrise Arc”, “Cosmic Grapes”, “Firely Sparkle”, “Cosmic Gems”, and so on. These galaxies typically show five to ten clusters each, with half-mass radii of ~ 10 pc (1–100 pc), stellar masses of $\sim 10^{6.5} M_{\odot}$ ($10^5 - 10^9 M_{\odot}$), surface densities of $\sim 10^4 M_{\odot} \text{pc}^{-2}$ ($10^3 - 10^5 M_{\odot} \text{pc}^{-2}$), stellar ages of ~ 10 Myr (1–35 Myr), and relatively low metallicities of $< 0.1 Z_{\odot}$. They thus resemble in many ways the massive end of clusters predicted in the FFB scenario. The estimated overall stellar masses of the host galaxies are sometimes smaller than predicted by the original FFB model, but it is possible that the less massive clusters and the background stellar mass are not properly resolved and are therefore underestimated.

1.3. Black Hole Growth

Another central issue in the origin of LRDs is the rapid growth of super-massive central black holes (SMBHs). A feasibility study (A. Dekel et al. 2025b) indicates that the FFB scenario may provide a natural setting for such a black hole growth. The scenario involves the formation of seed BHs, of $\sim 10^4 M_{\odot}$, by sped-up core collapse in the young, rotating FFB star-clusters (J. Spitzer & M. H. Hart 1971; I. Hachisu 1979; S. F. Portegies Zwart et al. 2004; B. Devecchi & M. Volonteri 2009; H. Katz et al. 2015; A. Rantala et al. 2024). It is followed by migration of the clusters and BHs to the galactic-disk centers, driven by dynamical friction and two-body segregation that act on the clusters and the BHs. For the BH seeds to merge into SMBHs that are retained in the galaxy centers, the merger remnants have to overcome the bottleneck introduced by gravitational-wave (GW) recoils (F. Pretorius 2005; M. Campanelli et al. 2006; J. G. Baker et al. 2006). The ejection velocities in the case of BHs with comparable masses and non-negligible misaligned spins, as expected in galactic disks that are not unrealistically cold, are typically on the order of several hundred km s^{-1} . These are larger than the escape velocities of $\sim 200 \text{ km s}^{-1}$ expected in the typical cosmic-dawn galaxies produced in the FFB phase.

The lesson from the analysis of A. Dekel et al. (2025b) is that a necessary condition for the growth of the central SMBH is a deepening of the central galactic potential well. This turns out to be a natural result of wet compaction events (see below). Beyond overcoming the GW recoils, such a deepening of the potential well would prevent suppression of the dynamical-friction-driven inspiral into the galactic center by core stalling (J. I. Read et al. 2006; T. Goerdt et al. 2006; K. Kaur & S. Sridhar 2018; U. Banik & F. C. van den Bosch 2021). It could also assist in overcoming the final parsec problem (M. C. Begelman et al. 1980) by providing central

gas. Finally, it would stop the off-center wandering of the SMBH, locking it to the galaxy center (S. Lapiner et al. 2021).

1.4. Wet Compaction Events

Both cosmological simulations (e.g., A. Zolotov et al. 2015; S. Lapiner et al. 2023) and observations (e.g., G. Barro et al. 2013; P. G. van Dokkum et al. 2015; G. Barro et al. 2017; A. de Graaff et al. 2024) reveal that most galaxies undergo throughout their histories gas-rich (“wet”) compaction events into compact starbursts (termed “blue nuggets”). These events induce major transitions in the galaxy properties, and in particular trigger quenching of star formation into “red nuggets”. As discussed in S. Lapiner et al. (2023), the compaction processes are due to drastic angular-momentum losses. About half of these are caused by mergers and the rest by colliding counter-rotating streams, recycling fountains from the galactic disks, disk-instability-driven radial transport (A. Dekel & A. Burkert 2014) and possibly other mechanisms.

The major compaction events, those that trigger a decisive long-term quenching process and a transition from central dark-matter to baryon dominance, tend to occur near the golden mass, halos of masses $10^{11} - 10^{12} M_{\odot}$ (A. Dekel et al. 2019) at all redshifts. This is seen in cosmological simulations (M. Tomassetti et al. 2016) and in machine-learning-aided comparisons to observations (M. Huertas-Company et al. 2018). This preferred mass scale for major compaction events seems to be due, at least partly, to the physical processes of supernova feedback and hot circum-galactic medium (CGM), which tend to suppress compaction attempts at lower and higher masses, respectively. At cosmic dawn, the FFB halos are indeed of masses $\sim 10^{11} M_{\odot}$, in the vicinity of the golden mass, and they correspond to high-sigma peaks of $> 4\sigma$ (A. Dekel et al. 2025a), which tend to have more frequent and stronger compaction events due to multiple colliding streams with low angular momentum (Y. Dubois et al. 2012).

The compaction events trigger a sequence of morphological changes, which may be relevant both to the beginning and the end of the LRD phase. The compaction events drive central starbursts in the form of blue nuggets, followed by inside-out quenching to quiescent red nuggets, as a result of gas depletion due to star formation and the associated outflows (S. Tacchella et al. 2016b,a).

We use here cosmological simulations, utilizing a variety of codes and physical models at different epochs, to quantify the compaction-driven growth of compact, massive, central stellar clusters, beyond their growth by dry mergers of clusters. These central clusters could plausibly be identified with the stellar systems of LRDs, and could possibly increase the escape velocities to the level that is required for retaining the SMBHs at the centers against GW recoils.

1.5. Disappearance of LRDs

Subsequently, the compaction events lead to the formation of extended gas disks and rings, fueled by new incoming cold streams (S. Tacchella et al. 2016a; A. Dekel et al. 2020b). The compact massive nuggets (or bulges) stabilize the disks/rings against gravitational instability. This suppresses star formation in the outskirts (“morphological quenching”, M. Martig et al. 2009) and limits the rate of instability-driven radial gas transport toward the center, maintaining long-lived, star forming disks/rings (A. Dekel et al. 2020b; D. Dutta Chowdhury et al. 2024). These disks/rings tend to appear above the golden mass.

Such a disk would mark the end of a naked red nugget, or LRD, by adding a blue extended envelope. Indeed, using JWST/CEERS observations, J.-B. Billand et al. (2025) identify a population of galaxies at $z < 4$ that could represent the descendants of LRDs after developing blue peripheries of recently formed young stars around their red cores. The consistency is in terms of the properties of the red core and the number densities of the populations.

It turns out that long-lived extended disks are coincidentally expected to be favored above the same golden mass of $M_{\text{vir}} \sim 10^{11} M_{\odot}$ due to the fact that merger-driven disk flips become less frequent than the disk orbital time above this mass at all redshifts (A. Dekel et al. 2020a). We thus expect that LRDs will disappear once their host halo masses exceed $M_{\text{vir}} \sim 10^{11} M_{\odot}$. This turns out to be the mass of 2-sigma peak halos at $z \sim 4$.

1.6. Outline

A parallel study (Dutta Chowdhury et al. in preparation) is underway, which performs N-body simulations of the dry evolution of a galactic disk with FFB clusters and BH seeds, and investigates the resultant compact central star cluster and the growth of a SMBH.

The current paper is organized as follows. In §2 we summarize the properties of fiducial cosmic-dawn disks and the FFB clusters in them. In §3 to §5 we evaluate analytically the possible formation of LRD-like compact central stellar clusters via dry inward migration and mergers of FFB clusters: in §3 we estimate the migration timescales for two-body segregation and dynamical friction, in §4 we evaluate the compactness of the merger-built central clusters, and in §5 we work out the mutual tidal effects of the clusters during the migration process. Then, in §6, we address the growth of SMBHs via mergers of BH seeds which are carried in by the migrating clusters, and highlight the need for further deepening of the central galactic potential wells in order to overcome SMBH ejection by GW recoils. In §7 we use a variety of cosmological simulations to study the deepening of the potential wells by wet compaction events due to wet mergers, and their contribution to the formation of compact central

stellar systems. In §8 we address the favored epoch, masses and abundance of LRDs. Finally, in §9, we summarize our results and conclude.

2. FFB CLUSTERS

To be used as an example in our estimates below, we recall the properties of a fiducial FFB galaxy at $z=9$ according to A. Dekel et al. (2023). The dark-matter halo virial mass, radius and velocity are

$$M_{\text{vir}} \simeq 6 \times 10^{10} M_{\odot} (1+z)_{10}^{-6.2}, \quad (1)$$

$$R_{\text{v}} \simeq 12.3 \text{ kpc } M_{\text{v},10.8}^{1/3} (1+z)_{10}^{-1}, \quad (2)$$

$$V_{\text{v}} \simeq 148 \text{ km s}^{-1} M_{\text{v},10.8}^{1/3} (1+z)_{10}^{1/2}, \quad (3)$$

where $M_{\text{vir}} \equiv 10^{10.8} M_{\odot} M_{\text{v},10.8}$ and $(1+z) \equiv 10(1+z)_{10}$. With a global star-formation efficiency of $\epsilon = 0.3\epsilon_{0.3}$ (Z. Li et al. 2024), the total stellar mass in the galactic disk, all initially consisting of clusters, is

$$M_{\text{d}} \simeq 3 \times 10^9 M_{\odot} \epsilon_{0.3}. \quad (4)$$

With a contraction factor (\sim halo spin parameter) $\lambda \equiv 0.025\lambda_{.025}$, the half-mass radius of the disk is

$$R_{\text{d}} \simeq 307 \text{ pc } \lambda_{.025}. \quad (5)$$

Within R_{d} , the dark-matter halo mass is roughly $M_{\text{halo}}(R_{\text{d}}) \simeq (R_{\text{d}}/R_{\text{v}})M_{\text{vir}} \simeq 1.6 \times 10^9 M_{\odot} \lambda_{.025}$. The stellar mass is comparable, $0.5M_{\text{d}} \simeq 1.5 \times 10^9 M_{\odot} \epsilon_{0.3}$. The total mass within R_{d} is therefore

$$M(R_{\text{d}}) \simeq 3 \times 10^9 M_{\odot}. \quad (6)$$

The circular velocity at R_{d} , due to the halo and added disk, is thus

$$V(R_{\text{d}}) \simeq \left(\frac{GM(R_{\text{d}})}{R_{\text{d}}} \right)^{1/2} \simeq 206 \text{ km s}^{-1}. \quad (7)$$

The FFB disk is predicted to consist of star clusters, in the mass range $10^4 - 10^7 M_{\odot}$. These limits are determined by the minimum mass shielded against feedback from earlier generations of clusters and by the Toomre mass, respectively (A. Dekel et al. 2023, §7). The cluster mass function can be approximated by $dN/dm \propto m^{-\alpha}$ with $\alpha \lesssim 2$. This is based on zoom-in cosmological simulations (N. Mandelker et al. 2014, 2017), and is a generic result in a supersonic turbulent medium (P. F. Hopkins et al. 2013; S. Trujillo-Gomez et al. 2019; M. Gronke et al. 2022). The typical radius of a $10^6 M_{\odot}$ clump is $R_{\text{c}} \sim 7 \text{ pc}$. The corresponding densities are on the order of $n \sim 3 \times 10^4 \text{ g cm}^{-3}$ and $\Sigma \sim 6 \times 10^3 M_{\odot} \text{ pc}^{-2}$, above the thresholds for FFB.

3. DRY MIGRATION OF CLUSTERS: TIMESCALES

A galactic disk that consists of star clusters, embedded in a dark-matter halo, will evolve by gravity into a central compact stellar cluster. This evolution can be driven by two-body segregation and by dynamical friction. Using analytic toy models, we estimate here the timescales for these processes to bring the clusters from the disk half-mass radius R_{d} to the center. The migrating clusters will bring in with them the seed BHs that formed in the cluster centers (§6). These crude estimates are to be quantified using N-body simulations (Dutta Chowdhury et al., in preparation).

3.1. Two-body segregation

For a system of objects with a distribution of masses, two-body relaxation causes segregation, making the massive objects migrate to the center. Assuming that the clusters largely remain intact as point masses (see §5), and very crudely assuming a spherical system for this toy-model estimate, the segregation timescale at radial distance r can be approximated by (e.g. M. Giersz & D. C. Heggie 1994)

$$t_{\text{seg}} \sim \frac{0.17 N}{\ln(0.11 N)} t_{\text{dyn}}. \quad (8)$$

Here t_{dyn} is the dynamical time at r ,

$$t_{\text{dyn}} \simeq (4\pi G \rho)^{-1/2} \simeq \frac{r}{V}, \quad (9)$$

with ρ the density at r , and V the circular velocity there. The second equality is valid, e.g., for an isothermal sphere. In particular, we will refer to t_{dyn} at the stellar half-mass radius R_{d} . For equal-mass objects of mass M_{c} in a system of total mass M_{d} the number of objects relevant for two-body relaxation inside the half-mass radius is $N = 0.5 M_{\text{d}}/M_{\text{c}}$. For a multi-mass system, N should be replaced by $N = 0.5 M_{\text{c}}/M_{\text{c,max}}$, where $M_{\text{c,max}}$ is the typical mass of the most massive objects. This has been estimated by J. Spitzer & M. H. Hart (1971) and S. F. Portegies Zwart et al. (2004) for core collapse in a star cluster, where the stars are distributed according to a standard P. Kroupa (2001) initial mass function, namely of negative slope $\alpha = 2.3$ at large masses. This estimate has been confirmed in simulations (F. P. Rizzuto et al. 2021; A. Rantala et al. 2024). Similar estimates were obtained by S. F. Portegies Zwart & S. L. W. McMillan (2002); B. Devecchi & M. Volonteri (2009) as a function of the average object mass. For a population of clusters, the mass function is expected to be somewhat flatter, $dN/dM_{\text{c}} \propto M_{\text{c}}^{-\alpha}$ with $\alpha \lesssim 2.0$ (N. Mandelker et al. 2014, 2017), but we assume that the estimate of the effective N based on $M_{\text{c,max}}$ should be qualitatively valid.

For a fiducial FFB galaxy (§2), with a disk mass $M_{\text{d}} = 3 \times 10^9 M_{\odot}$ ($\times \epsilon_{0.3}$) and clusters of maximum mass $M_{\text{c,max}} \equiv 10^6 M_{\odot} M_{\text{c,max},6}$, the effective number of objects is $N = 3 \times$

$10^3 M_{c,\max,6}^{-1}$. With $V(R_d) \simeq 200 \text{ km s}^{-1}$ and $R_d \simeq 300 \text{ pc}$ ($\times \lambda_{.025}$), the dynamical time at R_d is

$$t_{\text{dyn}}(R_d) = \frac{R_d}{V} \sim 1.5 \text{ Myr}. \quad (10)$$

Then, from eq. (8), the segregation time, for $M_{c,\max} = 10^6 - 10^7 M_\odot$ respectively, is approximately

$$t_{\text{seg}} \sim (132 - 22) \text{ Myr}. \quad (11)$$

For given FFB halo properties, $t_{\text{seg}} \propto \epsilon_{0.3} \lambda_{.025}$.

Figure 1 shows the segregation timescale as a function of M_c for the fiducial FFB galaxy and clusters. This estimate of t_{seg} implies that the two-body segregation could bring the massive clusters from the disk half-mass radius to the galaxy center in a few orbital times, as long as a significant fraction of the clusters remain intact against mutual tidal stripping (see §5). We note that the cluster-resolving simulation by Chen et al. (in preparation) indeed reveals cluster mass segregation and inward migration on a timescale of $\sim 10 \text{ Myr}$.

3.2. Dynamical Friction

While dynamical friction is understood as a complex non-local process involving resonances (S. Tremaine & M. D. Weinberg 1984; K. Kaur & S. Sridhar 2018; U. Banik & F. C. van den Bosch 2021), a useful qualitative approximation can be obtained via the classical more local S. Chandrasekhar (1943) formalism, which sums up the two-body interactions between the moving massive object and the much less massive particles in the medium. The smooth component of the stellar disk, combined with the dark-matter halo, exert dynamical friction on the orbiting clusters, each hosting a black hole, which helps bringing them into the galaxy center. We next evaluate the contributions of the halo and the disk to the dynamical-friction-driven migration of the clusters.

3.2.1. Dynamical friction by the halo

Based on S. Chandrasekhar (1943), crudely applied to a spherical isothermal system, the dynamical-friction deceleration is

$$a_h \simeq F_h 4\pi G^2 \frac{\rho_h M_c}{V_{\text{rel}}^2}. \quad (12)$$

Here ρ_h is the dark-matter density in the halo at r , M_c is the object mass, and V_{rel} is the relative velocity between the object and the medium which we identify here with the total circular velocity given by $V^2 = GM(r)/r$. The factor F_h is of order unity, defined by $F_h \equiv \mathcal{B} \ln \Lambda$, where

$$\mathcal{B}(x) = \text{erf}(x) - \frac{2x}{\sqrt{\pi}} e^{-x^2}, \quad x = \frac{V_{\text{rel}}}{\sqrt{2}\sigma}, \quad \Lambda \sim \frac{M(r)}{M_c}, \quad (13)$$

with $\ln \Lambda$ the Coulomb logarithm. It is derived by integrating over the distribution of orbit impact parameters, between $b_{\max} \sim r$ and $b_{\min} \sim GM_c/V^2$.

Using $V^2 = GM(r)/r$, the deceleration becomes

$$a_h \simeq F_h 4\pi G \rho_h r \frac{M_c}{M(r)} = F_h \frac{V_h}{t_h(r)} \frac{M_c}{M(r)}. \quad (14)$$

The second equality is obtained by expressing the halo dynamical time t_h at r using eq. (10) for the quantities contributed by the halo alone, ρ_h and V_h .

Assuming that the halo mass and disk mass within R_d are comparable, $0.5 M_d \sim M_h(R_d)$, as in the fiducial FFB galaxy, we have $V_h \sim V/\sqrt{2}$ and $t_h \sim \sqrt{2} t_{\text{dyn}}$, so we finally estimate at R_d

$$a_h \sim \frac{F_h}{2} \frac{V}{t_{\text{dyn}}} \frac{M_c}{M(R_d)}. \quad (15)$$

Recall that V , t_{dyn} and M include the contributions from both the halo and the disk.

The migration timescale by dynamical friction from radius r to the center can be estimated as (J. Binney & S. Tremaine 2008, eq. 8.13)

$$t_{\text{df}} \simeq \frac{V}{2a} = \frac{V^2}{2r a} t_{\text{dyn}} = \frac{GM(r)}{2r^2 a} t_{\text{dyn}}, \quad (16)$$

where a is the dynamical-friction deceleration at r and V is the circular velocity there.

By inserting a_h from eq. (15) in eq. (16), we obtain for the timescale associated with the dynamical friction contributed by the halo at R_d , for a fiducial FFB galaxy where $0.5 M_d \sim M_h(R_d)$,

$$t_{\text{df,h}} \sim F_h^{-1} \frac{M(R_d)}{M_c} t_{\text{dyn}}. \quad (17)$$

For a numerical estimate, assuming a fiducial FFB galaxy, with $M(R_d) \simeq 3 \times 10^9 M_\odot$ and $t_{\text{dyn}} \simeq 1.5 \text{ Myr}$, consisting of clusters of mass $M_c = 10^6 M_\odot$, and assuming $F_h \sim 1$, we obtain

$$t_{\text{df,h}} \sim 4.5 \text{ Gyr } M_{c,6}^{-1}. \quad (18)$$

This is shown as a function of M_c in Figure 1. We learn that it is much longer than the timescale associated with two-body segregation, eq. (11), as well as with the timescale associated with dynamical friction by the disk once it has a significant smooth component (see next). We can thus practically neglect the contribution of dynamical friction by the halo.

3.2.2. Dynamical friction by the smooth disk

The dynamical friction exerted on an object rotating in a disk by the rotating background particles is expected to be more efficient than in a spherical system. As evaluated in A. Dekel et al. (2025b), this is largely because the relative velocity of the object with respect to the background particles, V_{rel} , is comparable to the velocity dispersion σ rather than the rotation velocity V . Since the dynamical-friction deceleration is proportional to V_{rel}^{-2} , the deceleration in a disk, of a density similar to the halo density, is expected to be larger by a factor

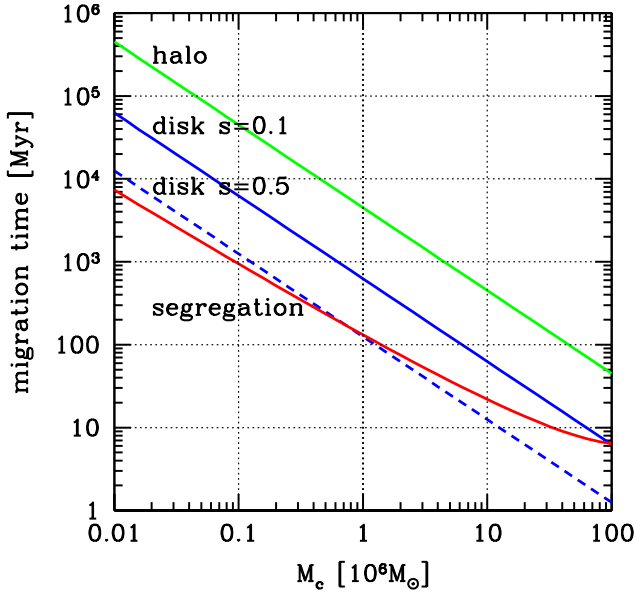


Figure 1. Migration timescales from the half-mass radius to the center as a function of cluster mass. The disk and cluster properties are the fiducial FFB values (§2). Shown are the timescales for two-body segregation (red, eq. (8)), for dynamical friction by a hot disk (eq. (22)) for a smoothed component fraction $s=0.1$ (solid blue) and $s=0.5$ (dashed blue), and for dynamical friction by the halo (green, eq. (17)). For the segregation M_c stands for the maximum cluster mass, while for the dynamical friction it is the mass weighted average cluster mass.

$(V/\sigma)^2$, with an additional contribution by a geometrical factor.

A. Dekel et al. (2025b, eqs. 19 and 21) evaluated the dynamical-friction deceleration in a disk to be

$$a_d \simeq F_d 8\pi G \Sigma'_s(r) r \left(\frac{M_c}{M(r)} \right)^\mu \left(\frac{R_d}{H_d} \right)^\nu. \quad (19)$$

For a kinematically hot thick disk (or when $M_c \ll M_d$), which is relevant at high redshifts, the power indices are $\mu=1$ and $\nu=2$. For a cold thin disk (or when M_c is not much smaller than M_d), they are $\mu=2/3$ and $\nu=1$. The ratio H_d/R_d is the relative thickness of the disk, which can be approximated by $H_d/R_d \sim \sigma/V$. The dependence of a_d on $(H_d/R_d)^2$ reflects the mentioned dependence on σ^{-2} rather than on V^{-2} . The factor F_d is of order unity; its value is uncertain and can be calibrated using simulations (e.g. A. Dekel et al. 2025b).

In eq. (19), $\Sigma_s(r)$ is the surface density of the smooth component of the disk, and $\Sigma'_s(r)$ is its radial derivative. For an order-of-magnitude estimate, the quantity $\Sigma'_s(r) r$ can be approximated by $\Sigma_s(r)$ in the main body of the disk. This is given that for an exponential disk they are equal at the exponential radius r_{exp} , and that the half-mass radius is in the same ballpark, $R_d \simeq 1.68 r_{\text{exp}}$. In the main body of the disk, we also crudely replace $\Sigma(r)$ with its average inside r , $\bar{\Sigma}(r)$, the latter being higher by 43% at r_{exp} for an exponential disk.

We assume that the smooth component of the disk mass at the time relevant for dynamical friction is a fraction s of the stellar disk mass,

$$M_{d,s} = s M_d, \quad (20)$$

which we apply within R_d . Then $\bar{\Sigma}_s = s \bar{\Sigma}$ for the disk, so eq. (19) becomes

$$a_d \simeq F_d 8\pi G s \bar{\Sigma}(r) \left(\frac{M_c}{M(r)} \right)^\mu \left(\frac{R_d}{H_d} \right)^\nu. \quad (21)$$

At the early stages s is small, as estimated analytically in §5 and by simulations in A. Dekel et al. (2025b), so the disk contribution to the dynamical friction is minor. As the migration continues, the clusters tidally strip each other outskirts to form a smooth stellar background that grows inside out from the galaxy central region on a timescale of several tens of Megayears, making the dynamical friction more effective. We adopt $s=0.5$ as the fiducial value, relevant for the masses within R_d after several tens of Megayears.

Translating the deceleration to a dynamical-friction timescale using eq. (16), and using $\bar{\Sigma}(R_d) = 0.5 M_d / (\pi R_d^2)$ in eq. (21), we obtain

$$t_{\text{df,d}} \simeq \frac{1}{8F_d} s^{-1} \left(\frac{M(R_d)}{M_d} \right) \left(\frac{M(R_d)}{M_c} \right)^\mu \left(\frac{H_d}{R_d} \right)^\nu t_{\text{dyn}}. \quad (22)$$

For a fiducial FFB galaxy, where $M(R_d) \sim M_d$, assuming $M_d = 3 \times 10^9 M_\odot$, $M_c = 10^6 M_\odot$, $t_{\text{dyn}} = 1.5 \text{ Myr}$, $s = 0.5$, $H_d/R_d = 1/3$ in a hot disk ($\mu=1$ and $\nu=2$), and $F_d = 1$, we finally obtain

$$t_{\text{df,d}} \sim 124 \text{ Myr } M_{c,6}^{-1}. \quad (23)$$

This is shown as a function of M_c for different values of s in Figure 1.

Comparing the dynamical-friction decelerations by the disk and by the halo, using eq. (21) and eq. (14), we obtain

$$\frac{a_d}{a_h} \simeq 2 \frac{F_d}{F_h} \frac{s \bar{\Sigma}(R_d)}{\rho_h R_d} \left(\frac{R_d}{H_d} \right)^\nu. \quad (24)$$

With $\rho_h r = \bar{\Sigma}_h(r)/4$ for an isothermal sphere, and $\bar{\Sigma}_h(R_d) = \bar{\Sigma}(R_d)$ for the fiducial FFB galaxy, this becomes

$$\frac{a_d}{a_h} \sim 8 \frac{F_d}{F_h} s \left(\frac{R_d}{H_d} \right)^\nu. \quad (25)$$

With $F_d = F_h$, $s = 0.5$, $R_d/H_d = 3$, and $\nu = 2$, the deceleration by the disk is larger than the halo contribution by a factor of 36. Even given the uncertainties in the numerical factors F , and the crude approximations made in the analysis, it is clear that, once s is a non-negligible fraction of unity, the halo contribution to the dynamical friction is negligible compared to the disk contribution.

We learn that, once s is a significant fraction of unity, the timescale for dynamical friction by the disk, as estimated for

a fiducial FFB galaxy in eq. (23), is comparable to the two-body segregation timescale, as estimated by eq. (11). Both are on the order of $100 \text{ Myr } M_{c,6}^{-1}$. Clusters more massive than $10^6 M_\odot$ can migrate inwards in less than 100 Myr. We therefore expect cluster migration and the emergence of a significant central stellar cluster on this timescale.

3.3. Migration summary

Figure 1 summarizes the different timescales for migration from the disk half-mass radius to the center as a function of cluster mass for typical FFB galaxies. They are computed for a fiducial FFB disk of clusters (§2). Shown are the timescales for two-body segregation (eq. 8), for dynamical friction by a hot disk (eq. 22, with $F_d = 1$) with a smoothed component fraction $s = 0.1$ and $s = 0.5$, and for dynamical friction by the halo (eq. 17, with $F_h = 1$). Note that in the segregation timescale M_c stands for the maximum cluster mass, while in the dynamical friction estimates it refers to a certain average cluster mass. We learn that the two-body segregation timescale dominates the migration. For $M_c \sim 10^6 M_\odot$ it is estimated to bring half the clusters to the center in ~ 100 Myr. Clusters of higher maximum mass of $\sim 10^7 M_\odot$ will get to the center in ~ 20 Myr. The dynamical friction by the disk operates on a longer timescale in the early stages of the migration when s is small. If and when the stripped mass into a smooth component reaches half the disk mass, $s \sim 0.5$ (see §5 for estimates of s), the dynamical friction timescale becomes comparable to the segregation timescale. The dynamical friction by the halo is estimated to provide a less important contribution, operating on a timescale of a few Gigayears.

Seed black holes that form at the centers of the clusters will be carried by the inspiraling clusters and brought to the center where they could be ready to merge. However, we note that according to A. Dekel et al. (2025b, §3, Fig. 2), the very massive clusters of $\sim 10^7 M_\odot$, unlike the $\leq 10^6 M_\odot$ clusters, are not expected to form black-hole seeds very efficiently. It is the clusters of $\sim 10^6 M_\odot$ that are more relevant for the BH growth (see §6).

The migration timescale of a few tens of Megayears is on the order of the duration expected for the FFB phase at cosmic dawn, and is much shorter than the ~ 1 Gyr period available for LRD formation at cosmic morning. We thus expect the onset of LRDs by dry migration and mergers to start soon after the end of the FFB phase at $z \sim 8$.

4. GROWTH OF A CENTRAL SYSTEM BY DRY MERGERS

We next estimate the compactness of the final central merger remnant, starting from a population of clusters, each with a given mass and radius, that migrate to the galaxy center and merge there. For each dry binary merger, we use the simple recipe by M. Covington et al. (2008), which has been

calibrated by a variety of binary merger simulations. They demonstrated that in a dry binary merger of systems of mass M_1 and M_2 with half-mass radii R_1 and R_2 , respectively, the final radius of the merger remnant R_f is well approximated by

$$\frac{(M_1 + M_2)^2}{2 R_f} = \frac{M_1^2}{2 R_1} + \frac{M_2^2}{2 R_2} + \frac{M_1 M_2}{R_1 + R_2}. \quad (26)$$

This equation reflects conservation of energy of virialized systems, with the addition of the mutual potential energy of the two systems when their centers are at a distance $R_1 + R_2$. Similar estimates were obtained by others (S. Cole et al. 2000; S. Hatton et al. 2003; S. Shen et al. 2003). For an equal-mass merger, with initial half-mass radii R_i , this gives

$$R_f = \frac{4}{3} R_i. \quad (27)$$

For more minor mergers, the growth of radius for a given growth of mass is smaller.

We “simulate” the growth of a central cluster by a sequence of binary mergers with incoming clusters. Each cluster is assumed to be of mass $M_c \equiv 10^6 M_\odot M_{c,6}$ and half-mass radius $R_c \equiv 7 \text{ pc } R_{c,7}$. The corresponding mean densities within R_c are

$$\rho_c = 1.54 \times 10^4 \text{ cm}^{-3} M_{c,6} R_{c,7}^{-3}, \quad (28)$$

$$\Sigma_c = 3.25 \times 10^3 M_{c,6} R_{c,7}^{-2}. \quad (29)$$

The escape velocity, $V_{\text{esc}}^2 = 2 V_c^2 = 2 G (0.5 M_c) / R_c$, is

$$V_{\text{esc}} = 25.3 \text{ km s}^{-1} M_{c,6}^{1/2} R_{c,7}^{-1/2}. \quad (30)$$

We denote the growing mass of the central cluster by M and its half-mass radius by R . The sequence of mergers is between the central cluster of mass $M_1 = M$ and an incoming cluster of mass $M_2 = M_c$. For comparison, we also test a sequence of equal-mass mergers, where $M_2 = M$ (which can be followed analytically using eq. (27)). In a merger, the mass M becomes $M_1 + M_2$, and the post-merger radius is given by eq. (26). Figure 2 shows the evolution of the central-cluster half-mass radius R and the mean densities within it as a function of the growing M . It also shows the escape velocity, $\sqrt{2} V(R)$, multiplied by an additional factor of $\sqrt{2}$ to account for a dark-matter halo of comparable mass within R .

The sequence of mergers with mass M_c and M leads to higher densities than the sequence with equal-mass mergers. For example, starting from $M_c = 10^6 M_\odot$ and $R_c = 7 \text{ pc}$, when the central mass M reaches $10^9 M_\odot$, its properties are

$$R = 62.7 \text{ pc}, \quad (31)$$

$$\rho = 2.14 \times 10^4 \text{ cm}^{-3}, \quad \Sigma = 4.05 \times 10^4 M_\odot \text{ pc}^{-2}, \quad (32)$$

$$V_{\text{esc}} = 378 \text{ km s}^{-1}. \quad (33)$$

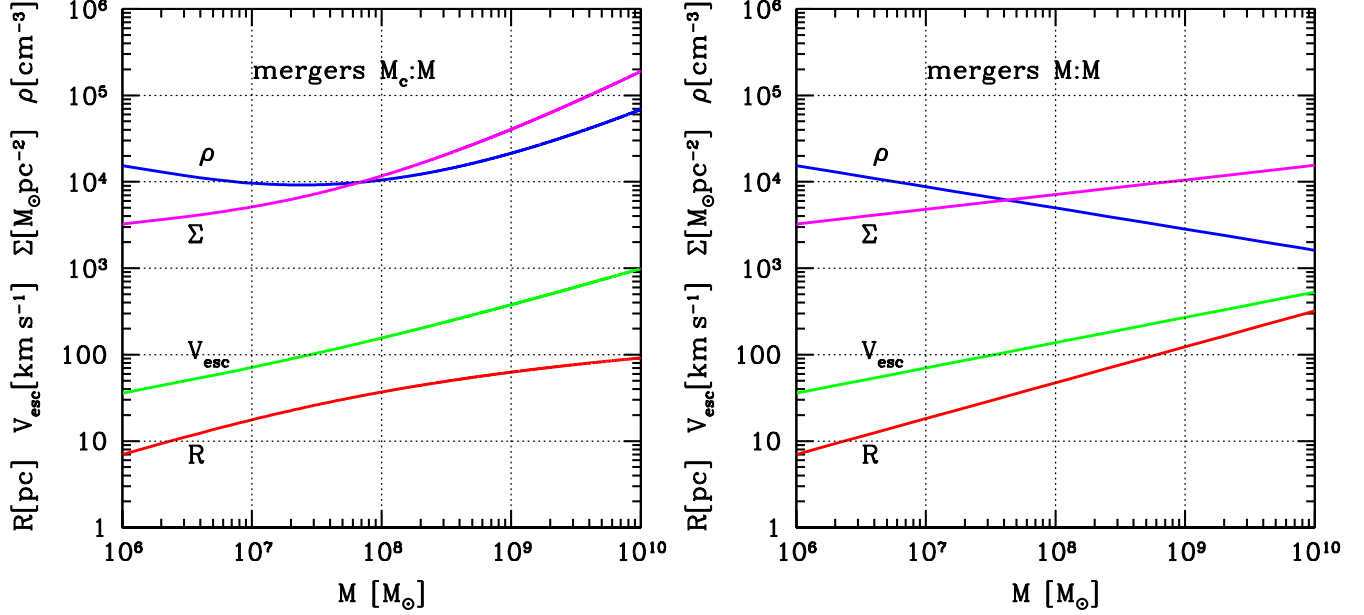


Figure 2. Evolution of central dry merger remnant. A sequence of mergers is followed using eq. (26). **Left:** the incoming mergers are of mass $M_c = 10^6 M_\odot$. **Right:** the incoming mergers are of mass M equal to the current central cluster. Shown are the half mass radius R , the corresponding 3D and surface mean densities within R , ρ and Σ , and the escape velocity (multiplied by $\sqrt{2}$ to account for a dark-matter halo and gas component).

The obtained central properties are similar when starting with more massive clusters of $M_c = 10^7 M_\odot$ and $R_c = 15$ pc.

We note that this estimated compactness is likely an overestimate because we ignored the mutual tidal stripping of the clusters, which could be significant after a few tens of Megayears (§5). On the other hand, even a small fraction of gas in the merging systems can enhance the compactness of the remnant, as found in M. Covington et al. (2008), and will be addressed in §7.

Dutta Chowdhury et al. (in preparation) performs N-body simulations of the dry evolution of a galactic disk with FFB clusters and BH seeds. In these simulations, after ~ 100 Myr, the average stellar surface density is $\Sigma \sim 10^6 M_\odot \text{pc}^{-2}$ within 10 pc and $\Sigma \gtrsim 10^4 M_\odot \text{pc}^{-2}$ within 100 pc. The corresponding escape velocities at these radii are high, 800 km s^{-1} and 600 km s^{-1} , respectively. These are comparable to our analytic estimates in Figure 2. We caution, however, that these simulations assume a rather top-heavy mass function for the clusters, with a flat slope of $\alpha = 1.4$ (instead of a more realistic ~ 2 slope) and maximum cluster mass as high as $10^8 M_\odot$ (compared to the FFB Jeans mass of $\sim 10^6 M_\odot$ and Toomre mass of $\sim 10^7 M_\odot$). This likely overestimates the inward migration efficiency and the resultant compactness of the central cluster. Furthermore, as mentioned, according to Fig. 4 of A. Dekel et al. (2025b), the clusters more massive than $\sim 10^6 M_\odot$ would find it difficult to form seed BHs in 3 Myr, before the death of the massive stars and the onset of feedback, such that the migration of the massive clusters may not be associated with the

growth of a SMBH (see §6). On the other hand, the estimated stellar masses of a few of the observed high-redshift clusters are possibly as high as $10^8 M_\odot$ (A. Claeysens et al. 2023; M. Messa et al. 2024), making the high end of the cluster mass function in the simulations acceptable in some cases. Also, certain simulations (M. C. Vergara et al. 2025a,b) indicate more efficient core collapse than in other simulations, possibly allowing seed BH growth in more massive clusters. The caveat is that these simulations assume unrealistic extremely compact initial clusters (see §6).

The estimated central radius and densities are close to the LRD stellar properties as crudely estimated for a hybrid LRD model of a stellar system with AGN. For a system of mass $M \equiv 10^9 M_\odot$ M_9 inside radius $R \equiv 100 \text{ pc}$ R_{100} , the LRD mean densities within R are

$$\rho \simeq 4.24 \times 10^4 \text{ cm}^{-3} M_9 R_{100}^{-3} \left(\frac{R}{H} \right)_3, \quad (34)$$

$$\Sigma \simeq 3.18 \times 10^5 M_\odot \text{pc}^{-2} M_9 R_{100}^{-2}, \quad (35)$$

and the escape velocity is

$$V_{\text{esc}} \simeq 299 \text{ km s}^{-1} M_9^{1/2} R_{100}^{-1/2}. \quad (36)$$

This escape velocity is actually comparable to the value of 291 km s^{-1} estimated for a fiducial FFB galaxy (eq. (7)). If this relatively moderate compactness is valid for LRDs, the dry evolution of clusters may be sufficient for reproducing the LRD properties. However, it is possibly not as high as

the value needed for retaining the SMBH after gravitational-wave recoils. According to Figure 4 below and A. Dekel et al. (2025b, Fig. 13), for a hot disk and a slope $\beta = 1.5$ for the BH mass function as they arrive at the center, the required escape velocity is $450\text{--}500\text{ km s}^{-1}$. Wet compaction events may be needed in order to increase the escape velocity to the required values (see §6 and §7).

5. TIDAL EFFECTS BY CLUSTER ENCOUNTERS

As the clusters orbit and spiral-in within the galactic disk, they gravitationally interact with each other, gain energy and lose mass by mutual tidal encounters. The binding energy and the mass that remains intact in the clusters during their inward migration are key for their migration efficiency, both by two-body segregation (§3.1) and by dynamical friction (§3.2). They are also important for the properties of the merger-driven central system, and for the ability of the clusters to keep the BHs in their centers during the migration. The mass that is stripped away is relevant for the dynamical friction exerted by the disk (§3.2.2). In order to address these issues, we crudely estimate the tidal evolution of cluster properties as a function of time.

5.1. The effects of a single encounter

We follow the analysis of hyperbolic tidal encounters by A. Dekel et al. (1980), based on L. Spitzer (1958). As long as the perturbing clusters orbit with relative velocities $V_p \sim 50\text{ km s}^{-1}$ or larger, while the internal velocities inside the clusters are only $V_c \sim 10\text{ km s}^{-1}$, one can adopt the *impulse approximation*, assuming that the stars in the victim cluster do not move appreciably as the perturbing cluster passes by. We consider a cluster of mass M_c and rms radius R_c ⁶. such that the internal rms velocity is $V_c^2 = GM_c/R_c$. The perturbing cluster is of mass M_p , moving at a velocity V_p relative to the victim cluster at closest approach that corresponds to an impact parameter p . In the *tidal limit*, where p is larger than R_c , the rms velocity increment in the cluster can be approximated by (L. Spitzer 1958)

$$(\Delta V_c)_{\text{tidal}} \simeq \left(\frac{2}{3}\right)^{1/2} \frac{2GM_p}{p^2 V_p} R_c. \quad (37)$$

The encounter can then be characterized by the dimensionless tidal parameter (A. Dekel et al. 1980, eq. 8)

$$\nu_{\text{tidal}} \equiv \frac{(\Delta V_c)_{\text{tidal}}}{V_c} \simeq 0.10 \left(\frac{4V_c}{V_p}\right) \left(\frac{2R_c}{p}\right)^2 \left(\frac{M_p}{M_c}\right). \quad (38)$$

We note based on experience that the impulse approximation and the tidal limit are the kind of assumptions that lead to

useful approximations even when they are only marginally valid, namely when V_p and p are not extremely large compared to V_c and R_c .

For a system with close-to-isotropic stellar orbits, A. Dekel et al. (1980) show that the relative energy gain in an encounter is dominated by the secular, second-order term in $\Delta V_c/V_c$.⁷ The energy gain of the bound system is calibrated by simulations to be (A. Dekel et al. 1980, eq. 10)

$$\frac{\Delta E_c}{E_c} \simeq -\frac{2}{3} \nu_{\text{tidal}}^2. \quad (39)$$

The associated relative mass loss is found there to be

$$\frac{\Delta M_c}{M_c} \simeq -\frac{2}{9} \nu_{\text{tidal}}^2. \quad (40)$$

Note that ΔE_c is positive and ΔM_c is negative.

Assuming that the cluster is in virial equilibrium both before and after the encounter, with corresponding radii R_c and $R_c + \Delta R_c$, masses M_c and $M_c + \Delta M_c$, and circular velocities V_c and $V_c + \Delta V_c$, one can write

$$1 + \frac{\Delta R_c}{R_c} = \frac{1 + \Delta M_c/M_c}{1 + \Delta E_c/E_c}, \quad (41)$$

$$\frac{\Delta V_c^2}{V_c^2} = \frac{\Delta E_c}{E_c}. \quad (42)$$

Using eq. (39) and eq. (40), and assuming $\nu_{\text{tidal}} \ll 1$, we obtain

$$\frac{\Delta R_c}{R_c} \simeq \frac{4}{9} \nu_{\text{tidal}}^2, \quad (43)$$

$$\frac{\Delta V_c^2}{V_c^2} \simeq -\frac{2}{3} \nu_{\text{tidal}}^2. \quad (44)$$

Thus, the energy, mass, radius and circular velocity of a cluster change as a result of the encounter by a multiplicative factor $[1 - (2/3)\nu_{\text{tidal}}^2]$, $[1 - (2/9)\nu_{\text{tidal}}^2]$, $[1 + (4/9)\nu_{\text{tidal}}^2]$, and $[1 - (2/3)\nu_{\text{tidal}}^2]^{1/2}$, respectively.

A caveat of the above analysis may refer to the assumption of tidal limit, in cases where p is not sufficiently large compared to R_c . We learn from A. Dekel et al. (1980) that for inter-penetrating, more head-on collisions, the more direct velocity increment is $(\Delta V_c)_{\text{direct}} \propto GM_p/(pV_p)$, such that $\nu_{\text{tidal}} \propto (pV_p)^{-1}$ and the actual mass loss is at a lower rate, only 1/20 of the bound energy change. In this case our estimate of mass loss based on the tidal limit could be an over-estimate of the actual mass loss. Nevertheless, we find in Figure 3 below that the tidal limit is expected to be valid in the fiducial circumstances studied.

⁶ For this toy-model estimate we do not distinguish between the rms radius and the half-mass radius.

⁷ The first order term, proportional to $\langle V_c \cdot \Delta V_c \rangle$, is expected to vanish for an isotropic system due to the symmetry between ingoing and outgoing stars, but it can become important if radial orbits dominate.

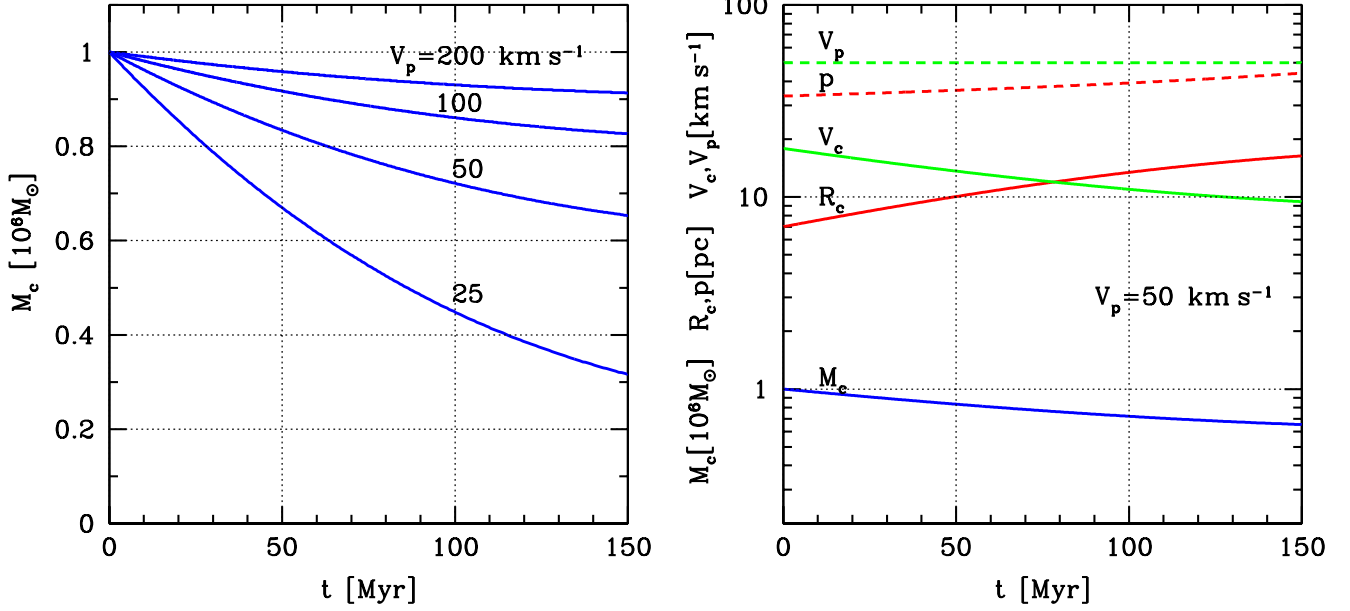


Figure 3. Evolution of clusters in a sequence of mutual tidal encounters assuming the impulse approximation and the tidal limit. **Left:** Tidal mass loss, for clusters of initial mass $M_c = M_p = 10^6 M_\odot$ and radius $R_c = 7$ pc, for different values of relative velocities V_p . The clusters largely remain in tact during the migration time of ~ 100 Myr, while a non-negligible smooth component develops for $V_p > 100$ km s^{-1} . **Right:** Evolution of cluster mass M_c (blue), radius R_c (red), and circular velocity V_c (green), compared to impact parameter p (dashed red) and relative velocity V_p (dashed green, assumed here to be 50 km s^{-1}). The validity of the impulse approximation and the tidal limit are indicated by $V_p > V_c$ and $p > R_c$, respectively.

As mentioned in an earlier footnote, another caveat that should be mentioned for completeness is that for clusters that happened to have more radial stellar orbits, the mass loss would be dominated by the first-order term in $\Delta V_c/V_c$ rather than by the second-order term. This is estimated in A. Dekel et al. (1980) to be $\Delta M_c/M_c \simeq -0.5 v_{\text{tidal}}$, such that the mass loss per encounter could be larger by an order of magnitude. We note, however, that the situation of radial orbits is unlikely, given that the FFB clusters form by fragmentation of a rotating disk, and are thus dominated by circular stellar orbits (D. Ceverino et al. 2012).

5.2. Evolution under a sequence of encounters

We next “simulate” a sequence of binary encounters based on the effects of a single encounter as estimated above. In order to relate the sequence of encounters to time, we estimate the time interval between successive encounters as

$$\Delta t = (n_p \sigma V_p)^{-1}. \quad (45)$$

Here the number density of clusters is

$$n_p = \frac{N_p}{\pi R_d^2 2H_d}, \quad (46)$$

where the initial total number of clusters within the half mass radius is

$$N_p = \frac{0.5 M_d}{M_p}, \quad (47)$$

and M_d , R_d and H_d are the mass, half-mass radius and half thickness of the disk of clusters, respectively. The cross section for an encounter is assumed to be

$$\sigma = \pi p^2. \quad (48)$$

The impact parameter is crudely assumed to be the mean separation of neighboring clusters, namely

$$p = N_p^{-1/3} \left(\frac{\pi 2H_d}{R_d} \right)^{1/3} R_d. \quad (49)$$

We consider the relative velocity V_p to be an input parameter whose value is very uncertain. It depends on the circular velocity, which may increase by contraction and slow down during the inward migration, developing a strong dependence on distance from the center. The value of V_p will affect the changes per encounter as $v_{\text{tidal}}^2 \propto V_p^{-2}$, but will counter-affect the encounter rate as $\propto V_p$. The fiducial FFB circular velocity is ~ 200 km s^{-1} , but the relative velocities V_p in the rotating disk are likely to be on the order of the velocity dispersion, which is smaller than the circular velocity by a factor of $H_d/R_d \sim 1/3$, namely $V_p \sim 67$ km s^{-1} . The velocity V_p may become even smaller after the inspiraling clusters slow down by dynamical friction and merging as they approach the center. On the other hand, the galaxy circular velocity may become higher than 200 km s^{-1} , either by a factor of order two due to the dry formation of a central cluster (§4) or possibly

by a larger factor due to wet compaction events (§7). This increase in circular velocity may compensate for the slow down of V_p , leaving fiducial values of $V_p \sim 50 - 100 \text{ km s}^{-1}$ but with a large uncertainty.

The relevant number of clusters N_p will decrease with time as the clusters gradually migrate and merge into the central cluster. We crudely assume that the disk of clusters is practically evacuated on a timescale that is twice the timescale associated with the inward migration by two-body segregation from R_d to the center. For a fiducial FFB galaxy and clusters of $10^6 M_\odot$ we estimated in eq. (11) $t_{\text{seg}} \approx 132 \text{ Myr}$. We very crudely adopt for $t < 2t_{\text{seg}}$ a linear decline of

$$N_p = N_p(t=0) \left(1 - \frac{t}{2t_{\text{seg}}}\right). \quad (50)$$

Before each encounter, we re-compute N_p by eq. (50). The impact parameter p is increased in proportion to $N_p^{-1/3}$ according to eq. (49). Then n_p and σ in eq. (45) are changed accordingly following eq. (46) and eq. (48). We equate M_p with the current M_c , and keep V_p constant.

Figure 3 shows the resultant time evolution of the cluster properties in a sequence of encounters where each encounter causes changes based on eq. (40), eq. (43) and eq. (44). Focusing on the mass loss, and recalling the uncertainty associated with the value of V_p , the left panel refers to different values of V_p from 200 km s^{-1} to 25 km s^{-1} . The right panel also shows the increase of R_c and decrease of V_c in comparison with p and V_p , for $V_p = 50 \text{ km s}^{-1}$. The fact that V_p is significantly larger than R_c indicates that the impulse approximation is a useful approximation. The fact that p is significantly larger than R_c indicates that the tidal limit is a useful assumption. We recall that if there were a significant inter-penetration, the effects deduced from the tidal limit would have over-estimated the actual effects.

We learn from Figure 3 that for $V_p \geq 100 \text{ km s}^{-1}$ the tidal effects are weak. Even for a relative velocity as low as $V_p \sim 25 \text{ km s}^{-1}$, a significant fraction of the mass is still bound to the clusters after the typical migration time of $\sim 100 \text{ Myr}$. The survival of bound clusters indicates that our estimated migration timescales (§3) and merger-driven central cluster properties (§4) can serve as reliable toy-model crude estimates.

The complementary non-negligible fraction of the mass at $\sim 100 \text{ Myr}$ is in a stripped, smooth, stellar disk capable of exerting dynamical friction as assumed in §3.2.2. This will accelerate the inward migration rate that is driven by two-body segregation, especially at its late stages.

The estimated mass loss in Figure 3 is in the ball park of the findings in an N-body simulation (A. Dekel et al. 2025b, Figs. 5 and 6).

6. BLACK HOLE GROWTH

As described in A. Dekel et al. (2025b), based on several other studies, the FFB clusters of $\sim 10^6 M_\odot$ at cosmic dawn are natural sites for the formation of BH seeds of $\sim 10^4 M_\odot$ via rapid core collapse to a central very massive star (VMS). The core collapse is sped up to $< 3 \text{ Myr}$ by two mechanisms. First, *gravo-thermal* instability (D. Lynden-Bell & R. Wood 1968), that is enhanced by two-body segregation in the presence of young massive stars (J. Spitzer & M. H. Hart 1971; I. Hachisu 1979; S. F. Portegies Zwart & S. L. W. McMillan 2002; S. F. Portegies Zwart et al. 2004; B. Devecchi & M. Volonteri 2009; H. Katz et al. 2015; F. P. Rizzuto et al. 2021; A. Rantala et al. 2024). Second, *gravo-gyro* instability (I. Hachisu 1979, 1982; A. Ernst et al. 2007; E. Kim et al. 2008; J. Hong et al. 2013; A. W. H. Kamlah et al. 2022), due to rotational support of the clusters in the galactic disk configuration (D. Ceverino et al. 2012). It has been estimated (A. Dekel et al. 2025b, Fig. 4) that BH seeds are expected to form efficiently in FFB clusters of $\sim 10^6 M_\odot$ and less. Formation of BH seeds in $\sim 10^7 M_\odot$ clusters, the estimated Toomre mass in FFB galactic disks, is likely to be efficient only if the stellar IMF is very top-heavy. This is because, otherwise, the core collapse in these clusters is expected to take more than 3 Myr , allowing the massive stars to die and stop contributing to the speed up of core collapse. Supernova feedback that turns on after 3 Myr may suppress the core collapse even further. We thus assume hereafter that the fiducial clusters which carry massive BH seeds are of $\sim 10^6 M_\odot$.

We note that N-body simulations of clusters (M. C. Vergara et al. 2025a,b) indicate core collapse to a VMS and possibly to a massive seed BH which is more efficient than in the other simulations mentioned above. These results, if extrapolated to clusters more massive than the $\sim 10^5 M_\odot$ simulated, may apparently allow BH seed growth also in massive clusters. However, the initial clusters assumed in these simulations are extremely compact, with unrealistically small half-mass radii of $(0.005 - 0.05) \text{ pc}$.

As estimated in §3, as long as the clusters are largely intact (see simulations in A. Dekel et al. 2025b, Fig. 5), the cluster migration inwards in the galactic disk can bring a significant fraction of the stellar mass into a central compact cluster in $\sim 100 \text{ Myr}$. The clusters should carry the BH seeds with them, bound by the cluster potential wells. Based on Figure 3, V_c is expected to be reduced by tidal encounters during the migration by only a factor of order two until they merge with the central cluster, likely keeping the clusters sufficiently bound for carrying the BHs with them. The cluster migration thus assists the BH migration into the center where they can merge into a SMBH, making the migration more efficient than assumed for naked BHs in A. Dekel et al. (2025b).

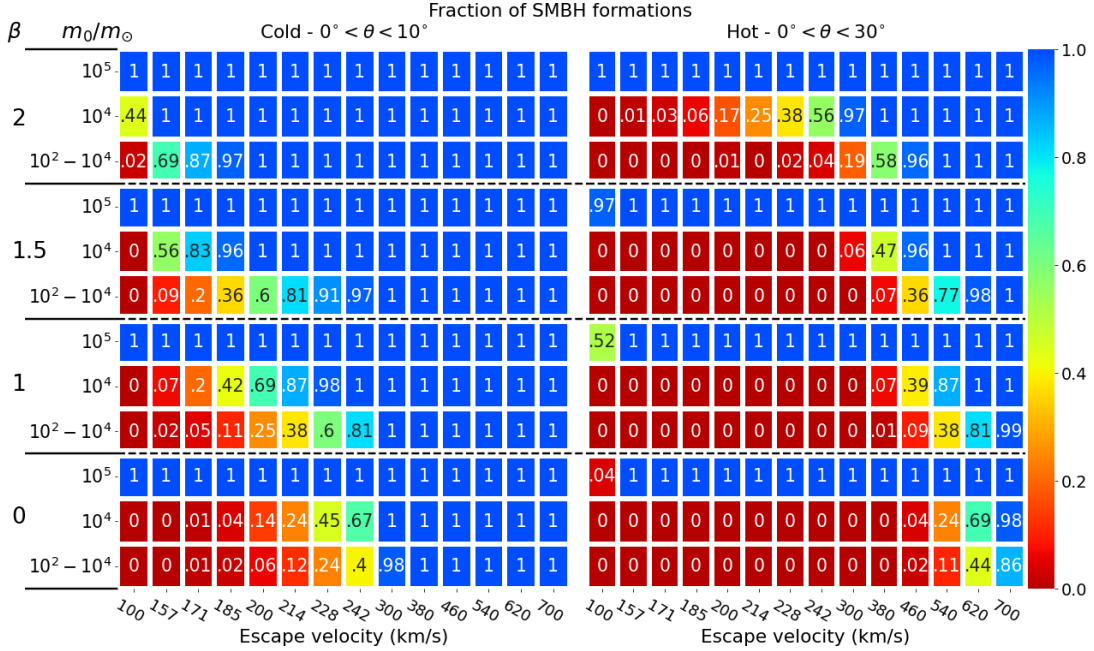


Figure 4. The recoil bottleneck of SMBH growth by BH mergers based on Monte Carlo simulations (A. Dekel et al. 2025b). The numbers (and colors) in each entry of the table represent the fraction of galaxies that allow SMBH growth exceeding $10^6 M_\odot$, as a function of the escape velocity from the galaxy V_{esc} . We consider the threshold escape velocity for retaining the SMBH to be given by a fraction of ~ 0.5 , namely near the entries colored yellow in the transition from red to blue colors. Shown are four cases of the BH mass-function slope β , with the fiducial case being $\beta = 1.5$. Also shown are cases of cold disk and hot disk, with spin-orbit misalignments $\theta = 0-10^\circ$ and $\theta = 0-30^\circ$, respectively. Within each of the eight sub-tables, shown are three cases of the initial primary BH mass, m_0 , which was either selected to be $10^5 M_\odot$ or $10^4 M_\odot$, or was drawn at random from the seed BH mass function in the range $(10^2-10^4 M_\odot)$. Focusing on the fiducial values adopted by A. Dekel et al. (2025b), of $\beta = 1.5$, a hot disk, and initial BH masses of $(10^2-10^4 M_\odot)$, we read that the threshold escape velocity is $V_{\text{esc}} \simeq 487 \text{ km s}^{-1}$. In comparison, the fiducial escape velocity of an FFB galaxy is $V_{\text{esc}} \sim 200 \text{ km s}^{-1}$ when ignoring compaction (§2), but it could rise to several hundred km s^{-1} after compaction (§7).

For the BH seeds to merge into massive BHs that are retained in the galaxy centers, the merger remnants have to overcome the bottle neck introduced by GW recoils (F. Pretorius 2005; M. Campanelli et al. 2006; J. G. Baker et al. 2006). The ejection velocities in the case of BHs with comparable masses and non-negligible misaligned spins, as expected in galactic disks that are not unrealistically cold, are typically of several hundred km s^{-1} . Based on the Monte Carlo simulations of sequences of BH mergers described in Section 5.5 (Figs. 10-13) of A. Dekel et al. (2025b), Figure 4 summarizes the required escape velocity for retaining the BH merger remnant in the galaxy. It is an expansion of the results summarized in Fig. 13 of A. Dekel et al. (2025b). The entries (and colors) represent the fraction of galaxies (out of 500 sequences) that allow SMBH growth exceeding $10^6 M_\odot$ (for a sequence of merging BHs of total mass $10^7 M_\odot$), as a function of the escape velocity from the galaxy V_{esc} and three other input parameters. We consider the threshold escape velocity for retaining the SMBH to be given by a fraction of ~ 0.5 of the sequences, namely the entries colored yellow in the transition from red to blue colors. Shown are four cases of the slope β of the seed BH mass function $dN/dm \propto m^{-\beta}$, as the BHs enter the central merger zone. Also shown are cases of

cold disk and hot disk, with spin-orbit misalignments drawn at random in the range $\theta = 0-10^\circ$ and $\theta = 0-30^\circ$, respectively. Within each of the eight sub-tables, shown are three cases of the initial primary BH mass m_0 , which was either selected to be $10^5 M_\odot$ or $10^4 M_\odot$, or was drawn at random from the seed BH mass function in the range $(10^2-10^4 M_\odot)$.

For no BH spins, or fully aligned spin and orbit, there is 100% growth in all cases considered (not shown in the figure). We read from Figure 4 that for a cold disk ($\theta = 0-10^\circ$), there is a significant fraction of growing SMBHs for V_{esc} values in the ballpark of 200 km s^{-1} , as in fiducial FFB galaxies. However, for a more realistic hot disk ($\theta = 0-30^\circ$), the threshold V_{esc} is in the range $240-640 \text{ km s}^{-1}$, well above 200 km s^{-1} . In particular, with the fiducial $\beta = 1.5$, a relatively hot disk, and a central primary BH of $10^2-10^4 M_\odot$, the required escape velocity for retaining the SMBH against recoil is $V_{\text{esc}} > 487 \text{ km s}^{-1}$. It could become even larger for a thicker disk with larger misalignments. This is significantly larger than the $V_{\text{esc}} \sim 200 \text{ km s}^{-1}$ expected in the typical cosmic-dawn galaxies produced in the FFB phase. The required escape velocity may also be larger than the value of $< 378 \text{ km s}^{-1}$ estimated in §4 for the buildup of central cluster by dry mergers. It seems that further deepening of the

central potential well is required in order to retain the BHs that are ejected by GW recoils. This could be a natural result of wet compaction events (see below).

Another requirement from the central potential well is that it is deep enough to prevent the BH from wandering around and lock it to the galaxy center. Using the NewHorizon simulations (Y. Dubois et al. 2021), it has been shown by S. Lapiner et al. (2021), e.g., in their Fig. 4 (illustrated in Figs. 3, C1 and C2), that pre-compaction the central BH is wandering at ~ 1 kpc about the galaxy center until a compaction event (at $z \sim 2-3$) locks it to the center. In these simulations, the post-compaction escape velocity at 1 kpc ($V_{\text{esc}} = \sqrt{2}V_{\text{circ}}$) ranges from 200 km s^{-1} (galaxy H51), to 500 km s^{-1} (H1, H6) to 1070 km s^{-1} (H18), to 1350 km s^{-1} (H3, H10) and to an extreme value of $3,400 \text{ km s}^{-1}$ (H2). The escape velocities that seem to be sufficient for bringing the BH to the center are typically half the above values. It does seem that in most cases a wet compaction is required for locking the BH to the center of the galaxy.

Wet compaction events could help the BH growth in two additional ways. First, the deepening of the potential well, associated with a steepening of the density profile, would be useful in preventing suppression of the dynamical-friction-driven inspiral into the galactic center by core stalling (J. I. Read et al. 2006; T. Goerdt et al. 2006; K. Kaur & S. Sridhar 2018; U. Banik & F. C. van den Bosch 2021). Second, the gas compaction could assist in overcoming the final parsec problem (M. C. Begelman et al. 1980) by providing central gas. A caveat is that wet compaction events bring in gas that could accrete onto the central BH and produce X-rays that are not seen in typical LRDs. Efficient gas depletion into stars and outflows should be considered in parallel with BH growth in order to explore this issue.

7. WET COMPACTION

Wet compaction events have been studied using a variety of cosmological simulations, using different codes and physical recipes, focusing on periods from cosmic dawn to cosmic noon, without and with black holes. For example, heavily used and currently available are the VELA and FirstLight suites of simulations utilizing the ART code (D. Ceverino et al. 2014, 2017), which explore cosmic morning with ~ 25 pc and ~ 13 pc resolution for the gas, respectively. We have just ran the MAGE simulations (Yao et al., in preparation), which focus on cosmic dawn with 10 pc resolution using the RAMSES code (R. Teyssier 2002). The NewHorizon simulation, which includes black holes, explores compactations at cosmic noon with a resolution ~ 40 pc using the RAMSES code. Unfortunately, these simulations do not yet resolve the FFB physical processes at cosmic dawn and the resultant clusters, which are key for the dry growth of the compact central clus-

ters and for the formation of BH seeds. These would require a resolution of order one parsec.

We analyze here sample galaxies from the VELA and MAGE simulations in order to evaluate the relative growth of compact central clusters by wet compaction events, and briefly refer to results from the NewHorizon simulations with BHs, but we cannot use these simulations to study the full combined effects of dry growth by cluster migration and global wet compaction events. This combination is likely to lead to higher compactness and escape velocities than are obtained by each process alone, but exploring the combined effects will have to await simulations of higher resolution, which should eventually also incorporate BHs. Preliminary results from the simulation with ≤ 3 pc resolution at cosmic dawn (Chen et al., in preparation) indicate that it begins to capture the combined effects of FFB clusters and compaction events, but we defer its analysis to future work.

7.1. Wet Compaction in VELA Simulations at Cosmic Morning

Wet compaction events in the VELA simulations and their major roles in transforming galaxy properties have been studied in a series of papers (A. Dekel & A. Burkert 2014; A. Zolotov et al. 2015; S. Tacchella et al. 2016a,b; M. Tomasetti et al. 2016; A. Dekel et al. 2020b, 2021) as summarized in S. Lapiner et al. (2023). These studies are based on the VELA suite of 32 zoom-in cosmological simulations (D. Ceverino et al. 2014) using the Adaptive Refinement Tree (ART) code (A. V. Kravtsov et al. 1997; D. Ceverino & A. Klypin 2009), with a maximum gas resolution of ~ 25 pc. Beyond gravity and hydrodynamics, the code incorporates the physics of gas and metal cooling, UV-background photoionization, stochastic star formation, gas recycling, stellar winds and metal enrichment. The main feedback processes are thermal supernova feedback and radiative pressure from massive stars, but no AGN feedback is included. Other limitations of these simulations are discussed in section 2 of S. Lapiner et al. (2023). The simulated galaxy properties are summarized in Table A1 of S. Lapiner et al. (2023). The halo masses at $z=2$ range from $10^{11}M_{\odot}$ to $10^{12}M_{\odot}$. Major compaction events occur in most of these galaxies at least once during cosmic morning, in the redshift range $z=2-6$ (S. Lapiner et al. 2023, Table A2).

Figure 5 shows face-on images of gas and stellar densities during the stages of a typical compaction event (in galaxy V07) at $z \sim 3.2$. It demonstrates the merger-driven gas contraction to a starbursting “blue nugget”, the following passive stellar evolution to a compact “red nugget”, and the subsequent formation of an extended star-forming gas disk and ring. This disk/ring, which is fed by incoming cold streams, is stabilized by the compaction-driven formation of a central mass (A. Dekel et al. 2020b). The red nugget may resemble

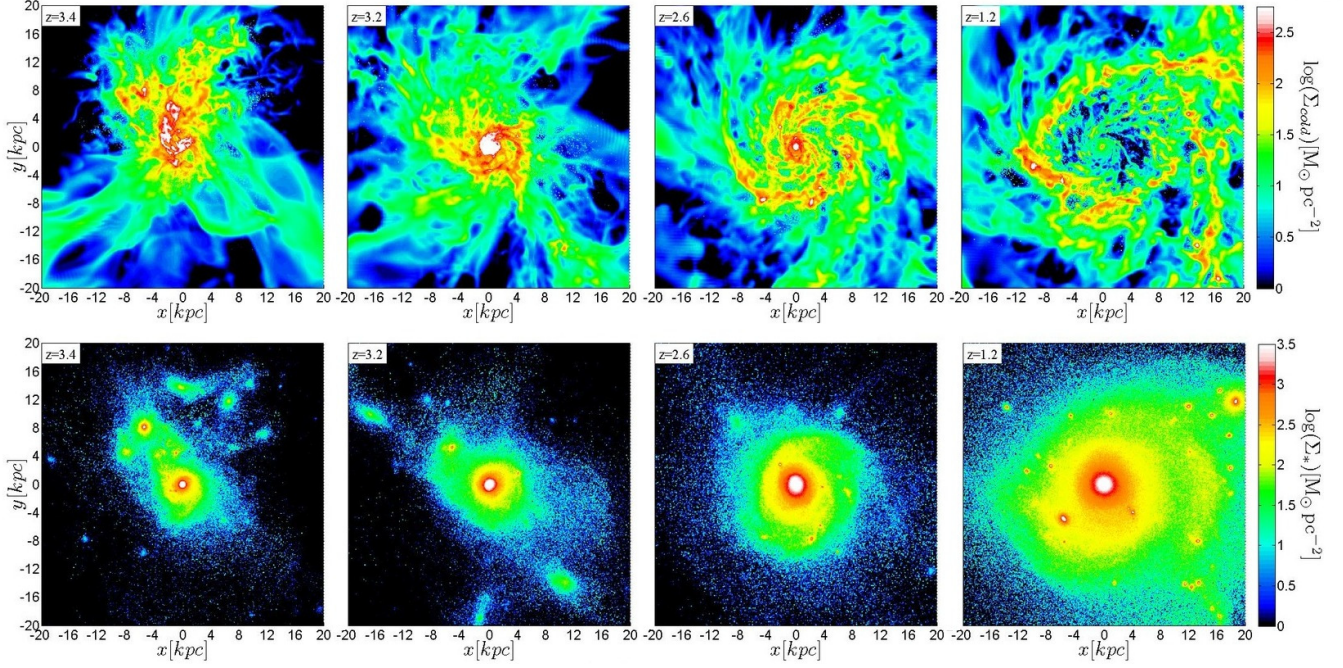


Figure 5. Wet compaction in a VELA simulation (V07). Shown is face-on density for gas (top) and stars (bottom). A merger causes gas compaction ($z = 3.4$), leading to a compact central star-bursting “blue nugget” ($z = 3.2$), which passively evolves to a long-lived “red nugget” (from $z = 2.6$ to $z = 1.2$ and on). The central mass allows the stabilization of an extended star-forming gas disk by incoming streams ($z = 2.6$), which evolves into an extended ring ($z = 1.2$). The red nugget resembles an LRD, while the emergence of an extended disk marks the end of the phase that is observationally identified as an LRD.

an LRD, while the appearance of an extended blue disk marks the end of the phase that is observationally identified as an LRD.

Figure 6 shows zoom-in images of post-compaction densities of another VELA galaxy (V12), at $z = 4$, demonstrating the formation of a star-forming nuclear disk. The mean surface density within 100 pc is $\sim 5 \times 10^5 M_\odot \text{pc}^{-2}$. This implies a mass of $3 \times 10^9 M_\odot$, and an escape velocity of $\sim 520 \text{ km s}^{-1}$.

At higher redshifts, for a given mass, the radius should scale as $(1+z)^{-1}$, and the 3D and 2D densities should scale as $(1+z)^3$ and $(1+z)^2$. As discussed below in §8, this naturally predicts a redshift dependence of the stellar-system compactness, and therefore of the abundance of LRDs as selected by their compactness, a dependence that is consistent with the observed trend (B. L. Jones et al. 2025).

Figure 7 quantifies the growth of compact central stellar clusters by wet compaction events in VELA cosmological simulations at cosmic morning (D. Ceverino et al. 2014; S. Lapiner et al. 2023). We analyze two example galaxies, V07 and V12, which show the most dramatic compaction events (at $z = 5-3$) among the 32 galaxies in the suite. We also analyze together the major compactations in the 16 most massive galaxies, selected by reaching a stellar mass above the median of $10^{10.06} M_\odot$ at $z = 2$. These galaxies are stacked together via time shifts that match the expansion factor $a(t)$ for each galaxy with the expansion factor a_{bn} that corresponds

to the peak of the major compaction event in terms of gas mass within 100 pc (the blue nugget phase). Shown are the medians and $\pm 1\sigma$ scatter.

The top panels show the evolution of mass within 100 pc for the stars, gas, and dark matter. While S. Lapiner et al. (2023) focused on the gas mass within 1 kpc, we here focus on the dramatic growth of inner stellar mass within $r < 100$ pc, relevant for LRDs. The middle panels show the average stellar density profiles $\bar{\rho}(<r)$ and $\bar{\Sigma}(<r)$ before and after the compaction. The bottom panels show the escape velocity at r , $V_{\text{esc}} = \sqrt{2}V_{\text{circ}}$, referring to the total mass of stars, gas and dark matter inside a sphere of radius r , which is relevant for the ability to retain the central BH against GW recoils. The selected pre-compaction and post-compaction times are marked in the top panels. For the stacked profiles, these times are taken to be at $\log(a/a_{\text{bn}}) = -0.22$ and $+0.06$.

We read from Figure 7 that the growth of stellar mass and densities within 100 pc during the compaction is by 2.9dex and 3.7dex for V07 and V12, and by 2.8dex for the stacked median. The growth of the escape velocity at 100 pc is by 1.4dex, 1.4dex, and 1.14dex, respectively. The post-compaction stellar mass within 100 pc reaches values $\sim 3 \times 10^9 M_\odot$. The 3D densities are $\bar{\rho} = 4 \times 10^4 \text{ cm}^{-3}$, $4 \times 10^4 \text{ cm}^{-3}$, and 10^4 cm^{-3} for the stacked median, and the surface densities are $\bar{\Sigma} = 5 \times 10^4 M_\odot \text{pc}^{-2}$, $5 \times 10^4 M_\odot \text{pc}^{-2}$, and $2 \times 10^4 M_\odot \text{pc}^{-2}$ for the median. The escape velocities at

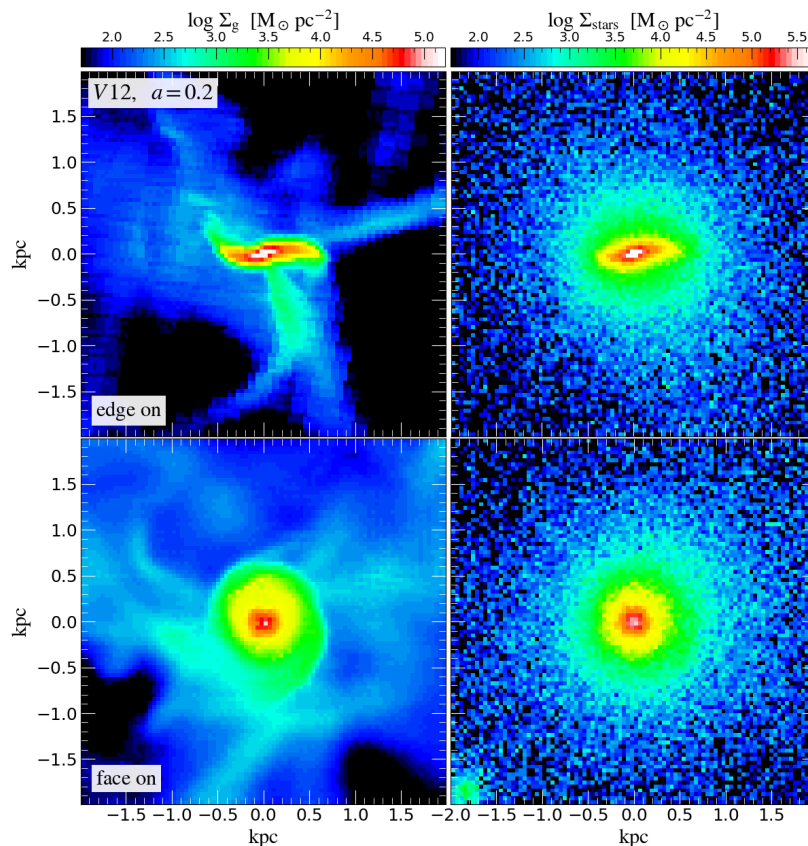


Figure 6. Nuclear disk as a result of wet compaction in a VELA simulation (V12) at $z=4$. The mean stellar surface density within a radius of 100 pc is in the ballpark of $\sim 5 \times 10^5 M_\odot \text{pc}^{-2}$. This implies a mass of $\sim 3 \times 10^9 M_\odot$, and an escape velocity $\sim 520 \text{ km s}^{-1}$.

100 pc become 540 km s^{-1} , 540 km s^{-1} , and 405 km s^{-1} for the attacked median, with the $+1\sigma$ value reaching 560 km s^{-1} .

We learn that the growth of stellar mass and densities within 100 pc due to the compaction event alone can be extremely large, by up to three orders of magnitude. This leads to central densities comparable to those of LRDs, and to escape velocities that are at the level required for retaining the SMBH against GW recoils. We assume that adding the effect of dry mergers of clusters could make the growth even more dramatic.

7.2. Wet Compaction in other simulations at Cosmic Morning

It is worth referring to other simulations that explore wet compaction events at cosmic morning. We refer in particular to the analysis of FirstLight simulations by P. Cataldi et al. (2025), and to the direct address of how a compaction leads to an LRD-like system by L. Mayer et al. (2024).

P. Cataldi et al. (2025) used 169 galaxies from the FirstLight suite of cosmological simulations (D. Ceverino et al. 2017) to study wet compaction events during cosmic morning, $z=5-9$ (compared to 32 galaxies with compaction events at $z=1-7$ in the VELA simulations). These simulations used the same ART code (D. Ceverino & A. Klypin 2009)

with a somewhat higher maximum resolution for the gas of $8.7-17$ proper parsecs (compared to ~ 25 pc in the VELA simulations). They focused on identifying compaction events based on the evolution pattern of the stellar half-mass radius (compared to evolution of gas and stellar mass in VELA). Their results largely strengthen the results from the VELA simulations (S. Lapiner et al. 2023). They find the favorable stellar mass range for compaction to be $M_* = 10^8 - 10^{10} M_\odot$ (P. Cataldi et al. 2025, Fig. 4), similar to the range found in VELA (S. Lapiner et al. 2023, Fig. 10). They find that the half-mass radius typically shrinks by $0.5-1.0$ dex during the compaction, sometimes down to 100 pc (P. Cataldi et al. 2025, Fig. 3), very similar to the finding in VELA (S. Lapiner et al. 2023, Fig. 14). Finally, they recover in a significant fraction of the galaxies a post-compaction increase in the half-mass radius, associated with the growth of an extended disk as seen in VELA, which we propose to identify with the end of the LRD phase (§8).

Appealing more directly to the formation of LRDs at cosmic morning, L. Mayer et al. (2024) studied the formation of a compact stellar system with a massive BH by a merger-driven compaction event in a cosmological simulation. Using the SPH code GASOLINE2 (J. W. Wadsley et al. 2017), with softening ~ 100 pc and maximum smoothing length of 7 pc,

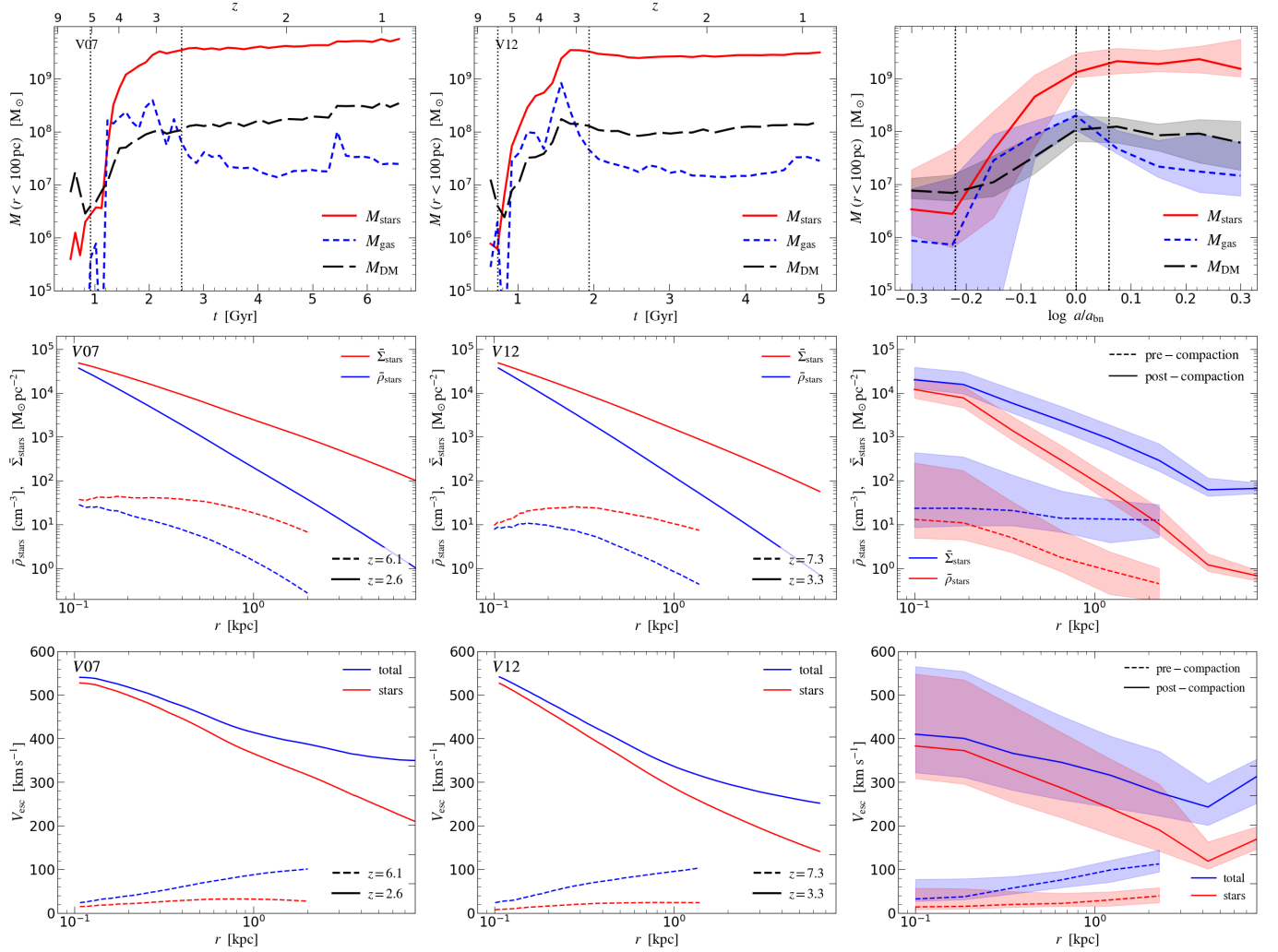


Figure 7. Growth of compact central stellar clusters by wet compaction events in VELA cosmological simulations at cosmic morning (D. Ceverino et al. 2014; S. Lapiner et al. 2023). Top: the evolution of mass within 100 pc for the stars (red), gas (short-dash blue) and dark matter (long-dash black). Middle: the average stellar density profiles at r before and after the compaction (dashed and solid). Bottom: the escape velocity at r referring to the total mass inside r . The left and middle panels each refer to a major merger event in galaxies V07 and V12, in which the most dramatic compactions are detected. The right panels refer to stacking the 16 most massive galaxies in the VELA suite each shifted horizontally such that the expansion factor $a(t)$ coincides at the time a_{bn} , corresponding to the peak of the compaction in terms of gas mass within 100 pc. Shown are the medians and $\pm 1\sigma$ scatter (shaded). For the stacked profiles, the pre-compaction and post-compaction times are taken to be at $\log(a/a_{\text{bn}}) = -0.22$ and $+0.06$. The growth of stellar mass within 100 pc during the compaction, and the corresponding densities, is typically by 3dex. The growth of the escape velocity is by 1dex to 1.5dex. The post-compaction stellar mass within 100 pc reaches $\sim 3 \times 10^9 M_{\odot}$ with densities $\bar{\rho} = (1-4) \times 10^4 \text{ cm}^{-3}$ and $\bar{\Sigma} = (2-5) \times 10^4 M_{\odot} \text{ pc}^{-2}$. The escape velocities at 100 pc become $(320-560) \text{ km s}^{-1}$.

they analyze a major-merger remnant at $z \simeq 8$. They find that about 10% of the gas in the host galaxy is compactified into a supermassive nuclear disk (SMD) of $\sim 10 \text{ pc}$ in size, a nuclear starburst and $3 \times 10^8 M_{\odot}$ in gas. Being bar unstable (L. Mayer et al. 2015; L. Mayer & S. Bonoli 2019; L. Zwick et al. 2023), they expect further contraction, which will become general-relativistic-unstable and form a supermassive BH of $10^6-10^8 M_{\odot}$ (M. Shibata & S. L. Shapiro 2002; M. Saijo & I. Hawke 2009; L. Zwick et al. 2023). In L. Zwick et al. (2025), they modeled the spectral features of an SMD of this sort, and showed that they match the spectra of LRDs, where the

V-shape arises from the superposition of two black bodies, and the Balmer line broadening is sourced by the intrinsic rotation of the SMD. This model may work without an AGN and with no X-rays. They argue that the number densities of LRDs are reproduced with mergers of galaxies more massive than $10^8 M_{\odot}$.

7.3. Wet Compaction in MAGE Simulations at Cosmic Dawn

In order to further explore the effects of wet compactions, with a different code and physical recipes and at earlier epochs

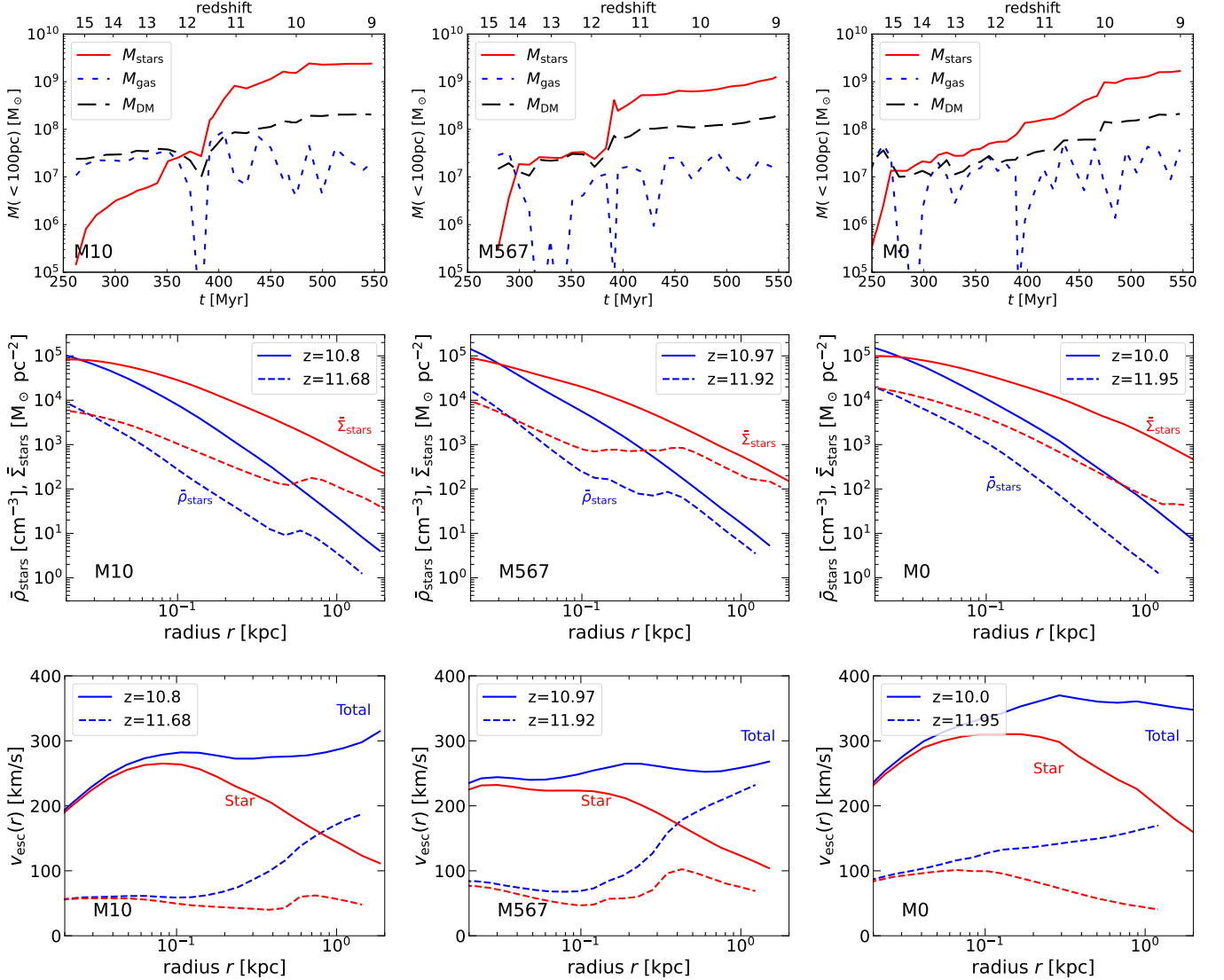


Figure 8. Growth of compact central stellar clusters by wet compaction events in MAGE cosmological simulations at cosmic dawn (Yao et al., in preparation). Shown are the evolution of mass within 100 pc for the stars, gas and dark matter (top), the average stellar density profiles at $< r$ before and after the compaction (middle), and the escape velocity at r referring to the total mass inside r (bottom). The left and middle panels each refer to a major merger event. The right panel refers to multiple merger events. The growth of stellar mass within 100 pc during the compaction, and the corresponding densities, is by 1.43dex, 1.30dex, and 0.9dex respectively. The growth of the escape velocity is by 0.70dex, 0.62dex, and 0.37dex.. The post-compaction stellar mass within 100 pc reaches $\sim 10^9 M_\odot$ with densities $\bar{\rho} = 7 \times 10^3 \text{ cm}^{-3}$, $5 \times 10^3 \text{ cm}^{-3}$, and 10^4 cm^{-3} , and $\bar{\Sigma} = 3 \times 10^4 M_\odot \text{ pc}^{-2}$, $2 \times 10^4 M_\odot \text{ pc}^{-2}$, and $3 \times 10^4 M_\odot \text{ pc}^{-2}$. The escape velocities at 100 pc become 280 km s^{-1} , 250 km s^{-1} , and 340 km s^{-1} .

corresponding to cosmic dawn, we analyze the compaction events in three galaxies from the MAGE suite of eleven zoom-in cosmological simulations (Yao et al., in preparation). This suite is utilizing the Adaptive Mesh Refinement (AMR) RAMSES code (R. Teyssier 2002) with 10 pc resolution for the gas. The physical models used are described in Z. L. Andalman et al. (2025). The galaxies M10 and M567 each happen to have a major merger (mass ratio ~ 1 and ~ 0.5 , respectively) at $z \sim 12-11$. The galaxy M0 has three successive mergers (of mass ratios $\sim 0.5, 0.6, 0.3$) at $z \sim 11.5-10$.

Two more galaxies from the suite of eleven (not shown here) have major mergers in the redshift range 13–9.

Figure 8 quantifies the growth of compact central stellar clusters by wet compaction events in the three MAGE simulations, along the lines of the analysis of VELA compaction events shown in Figure 7. The focus is on the mass, densities and escape velocity within 100 pc, relevant for LRDs.

We read from Figure 8 that the growth of stellar mass and densities within 100 pc during the compaction is by 1.4 dex, 1.3 dex, and 0.9 dex respectively. The growth of the

escape velocity is by 0.7 dex, 0.6 dex, and 0.4 dex. The post-compaction stellar mass within 100 pc reaches $\sim 10^9 M_\odot$ with a 3D density $\bar{\rho} = 7 \times 10^3 \text{ cm}^{-3}$, $5 \times 10^3 \text{ cm}^{-3}$, and 10^4 cm^{-3} for the three galaxies, and a surface density $\bar{\Sigma} = 3 \times 10^4 M_\odot \text{ pc}^{-2}$, $2 \times 10^4 M_\odot \text{ pc}^{-2}$, and $3 \times 10^4 M_\odot \text{ pc}^{-2}$, respectively. The escape velocities at 100 pc become 280 km s^{-1} , 250 km s^{-1} , and 340 km s^{-1} .

We learn that the growth of stellar mass and densities within 100 pc due to the compaction event alone can be (1–1.5) dex. This leads to central densities comparable to those of LRDs. The escape velocities are not by themselves at the level required for retaining the SMBHs against GW recoils. The lower escape velocities in MAGE compared to VELA is partly due to the fact that the MAGE galaxies at cosmic dawn are less massive than the VELA galaxies at cosmic morning. However, the growth of escape velocity by (0.4–0.7) dex in the MAGE galaxies does provide a significant deepening of the potential well. We assume that once combined with the growth induced by dry mergers of clusters it can bring the escape velocity to the level required for retaining the SMBHs against GW recoils.

8. EPOCH, MASS AND ABUNDANCE OF LRDs

If LRDs form along the lines of the scenario outlined above, one wishes to understand how it determines the epoch in which they are observed at cosmic morning, namely $z \simeq 4\text{--}8$, and their characteristic stellar masses of $\lesssim 10^9 M_\odot$.

The appearance of LRDs at $z \sim 8$ stems from the crucial need for star clusters in the proposed scenario. They are needed first of all for generating the BH seeds, and then for the efficient migration into the galaxy center where they can merge into a compact stellar system and allow the BH seeds to merge. These clusters naturally form in the FFB phase, typically prior to $z \simeq 8$ (A. Dekel et al. 2023, Fig. 6), and can thus lead to LRD formation soon after. The galactic stellar mass for a fiducial FFB galaxy is predicted to be $M_* \sim 2 \times 10^9 M_\odot \epsilon_{0.2} (1 + z_{\text{ffb}})_{10}^{-6.2}$, where $\epsilon \equiv 0.2 \epsilon_{0.2}$ is the global integrated star-formation efficiency, and $(1 + z_{\text{ffb}})_{10}$ refers to the redshift of the FFB phase. The total stellar mass in the clusters is thus predicted to be of order $\sim 10^9 M_\odot$, and smaller if the FFB phase occurred at $z > 9$ (A. Dekel et al. 2023, Fig. 6).

The apparent disappearance of LRDs from the observational samples towards cosmic noon and above a certain stellar mass may actually be a result of the same compaction events that are the second key element for LRD formation according to the proposed scenario. This is the post-compaction generic formation of an extended gaseous, star-forming disk or ring, as seen in Figure 5 and discussed in S. Lapiner et al. (2023). The shrinkage of this disk/ring is suppressed by the compaction-driven formation of a massive central object (A. Dekel et al. 2020b). This adds an extended blue envelope

around the red LRD, which makes it identified as non-LRD. It is ironic that the same compaction events that allow the appearance of LRDs with BHs eventually lead to their disappearance from the observed samples.

Observational support for the disappearance of LRDs by the formation of a blue envelope is provided by the detection of a population of galaxies with compact LRD-like central regions and star-forming blue envelopes at $z < 4$, using CEERS/JWST images (J.-B. Billand et al. 2025). The properties of these galaxies and their abundance seem to be consistent with being the post-LRD descendants of the LRDs. We note that, while this analysis assumed the stars-only model for LRDs and post-LRDs, namely very high stellar masses of $10^{10} M_\odot$ and surface densities of $10^7 M_\odot \text{ pc}^{-2}$, the match of these populations is not limited to this model. Similar results can be obtained when adopting the hybrid model of stars plus BHs both for the LRDs and the post-LRDs (David Elbaz, private communication).

Why would this scenario cause disappearance of LRDs after $z \sim 4$ and above stellar masses of $\sim 10^9 M_\odot$ (as deduced for LRDs with BHs)? It has been shown using analytic modeling and cosmological simulations that extended disks can be long-lived against spin-flips due to further major mergers once the halo mass is above $\sim 10^{11} M_\odot$ (A. Dekel et al. 2020a). For the typical SFE of ~ 0.1 at late cosmic morning, this implies a stellar mass above $\sim 10^9 M_\odot$. These halos represent two-sigma peaks in the density fluctuation field at $z \sim 4$, implying that more massive halos that can accommodate long-lived extended disks become more common after $z \sim 4$.

The number density of LRDs with BHs at cosmic morning is predicted to follow the number density of FFB galaxies at cosmic dawn, which is predicted to be $n \sim 10^{-5} \text{--} 10^{-4} \text{ Mpc}^{-3}$ (A. Dekel et al. 2025a). This stems from the prediction that cluster-dominated galaxies are a generic feature of the FFB phase, and because, as seen in the VELA simulations, every galaxy is expected to undergo at least one major compaction event during the ~ 1 Gyr period from cosmic dawn to cosmic morning. This predicted number density is in the ballpark of the observed abundance of LRDs (V. Kokorev et al. 2024; J. E. Greene et al. 2024; D. D. Kocevski et al. 2025).

The fact that at a given mass the expected radii scale with $(1 + z)^{-1}$ naturally lead to higher compactness at higher redshifts, and thus to an abundance of detected LRDs that is growing with redshift during cosmic morning, as indicated by observations (B. L. Jones et al. 2025).

9. CONCLUSION

We propose that the Little Red Dots, as detected in JWST observations, form naturally at cosmic morning, $z = 4\text{--}8$, as compact stellar systems with over-massive black holes. The two key elements in the proposed scenario are (a) the thousands of star clusters that form at cosmic dawn, $z > 8$, in a phase of feedback-free starbursts within the clusters, and

(b) wet compaction events that are associated with mergers or colliding cold streams. Our conclusions regarding four central elements of LRD formation can be summarized as follows.

9.1. Dry evolution of clusters

Investigating the dry evolution of the galactic disk of FFB clusters using analytic toy-modeling, we learned the following:

- The $10^6 M_\odot$ clusters allow efficient migration to the galaxy center, mostly by two-body segregation aided by dynamical friction against the disk, on a timescale of ~ 100 Myr (and shorter for more massive clusters).
- The clusters merge into compact central stellar clusters, containing $M \sim 10^9 M_\odot$ within radii of $R \sim 60$ pc, at mean densities of $\rho \sim 2 \times 10^4 \text{ cm}^{-3}$ and $\Sigma \sim 4 \times 10^4 M_\odot \text{ pc}^{-2}$. These are already in the ball park of the stellar systems deduced from observed LRDs using a hybrid model of stars and BHs.
- Mutual tidal stripping leaves most of the cluster mass intact such that it does not make a qualitative difference to the analysis. The part of the mass that is stripped into a smooth component allows the disk assist the migration by exerting dynamical friction on the clusters.
- Simulations of dry evolution of clusters with BHs (Dutta Chowdhury et al., in preparation) and high-resolution cosmological simulations at cosmic dawn (Chen et al., in preparation), reproduce the predicted rate of cluster migration and the formation of a massive, compact, stellar cluster.

9.2. Over-massive black holes

Regarding the growth of over-massive black holes in the LRDs, we find the following:

- A. Dekel et al. (2025b), following others, demonstrated that the FFB clusters are natural sites for the formation of BH seeds via rapid core collapse. The core collapse into a $10^4 M_\odot$ BH seed occurs in less than 3 Myr in young, rotating clusters of $\sim 10^6 M_\odot$. It is driven by gravo-thermal instability, which is governed by the massive stars that are still present during the first ~ 3 Myr. The core collapse is sped by gravo-gyro instability as long as the clusters are supported by rotation induced by their host disks.
- The migrating clusters then carry with them the BH seeds, making them ready for merging at the galaxy center into an over-massive BH.
- Extending the analysis of A. Dekel et al. (2025b), we showed that further deepening of the central potential well is needed in order to retain the SMBH in the galaxy against post-merger GW recoils, and in order to lock it to the galaxy center. This is higher than the compactness produced by dry migration of clusters, which is expected to lead to an escape velocity of $V_{\text{esc}} \sim 300 \text{ km s}^{-1}$.

9.3. Wet compaction events

We proposed that a natural solution to the GW recoil problem is provided by the common wet compaction events, triggered by mergers or other gaseous mechanisms that involve drastic energy and angular-momentum losses (S. Lapiner et al. 2023). In order to analyze the compaction-driven growth of a massive, compact, central stellar cluster, we used a variety of cosmological simulations, based on different codes and physical recipes, with compaction events that occur at redshifts from cosmic dawn to cosmic noon. We find the following:

- The relative increase of stellar mass within 100 pc in major compaction events can range from 0.5dex to more than 3dex. This by itself can lead to central stellar systems that match or exceed the compactness of LRDs as deduced from observations using the hybrid model of stars and BHs (e.g., F. Pacucci 2024; F. Pacucci & R. Narayan 2024).
- Major compactions typically boost the escape velocities by (0.5–1.5)dex. Adding to the growth of the central clusters by dry migration and mergers of clusters, we assume that the compactions can increase the escape velocities to the level required for retaining the SMBHs against GW recoils. Alternatively, these two mechanisms together could produce central stellar densities as high as required for LRDs without BHs.

9.4. Epoch, masses and abundance of LRDs

The period when LRDs are typically detected, $z = 8$ to 4, and their favorable stellar masses of $\lesssim 10^9 M_\odot$, can be related to the key elements of the scenario, namely clusters and compaction events, as follows:

- The LRDs appear after the formation of FFB clusters at cosmic dawn, typically at $z \sim 8$ (A. Dekel et al. 2023, 2025a), as they are crucial for the LRD formation. The fiducial stellar masses of FFB galaxies are predicted to be $\sim 10^9 M_\odot$.
- The LRDs escape being classified as LRDs by the natural development of post-compaction blue extended disks around the ‘‘LRD’’ cores. These disks/rings are fed by cold streams and are stabilized against contraction by the presence of compaction-driven central masses (A. Dekel et al. 2020b). The disks tend to survive subsequent mergers once the disk mass is above a threshold of $\sim 10^9 M_\odot$ (A. Dekel et al. 2020a). At $z \sim 4$, the dark-matter halos of corresponding masses become common two-sigma peaks of the density fluctuation field.
- The number density of LRDs with BHs at cosmic morning is predicted to follow the number density of FFB galaxies, $n \sim 10^{-5} - 10^{-4} \text{ Mpc}^{-3}$ (A. Dekel et al. 2025a), in the ball park of the observed abundance of LRDs. This is because cluster-dominated galaxies are a generic feature of the FFB phase and because every galaxy is expected to undergo major compaction events.

• The abundance of LRDs is expected to increase from $z \sim 4$ to $z \sim 8$ due to the scaling of size with $(1+z)^{-1}$ at a given mass, as observed (B. L. Jones et al. 2025).

The exploration of LRD formation by the combined effects of cluster migration and global compaction events will require challenging cosmological simulations with sub-parsec resolution that can capture the FFB physical processes in the clusters. They will have to rely on BH seed formation in the clusters, and simulate the migration and mergers of the clusters with BHs into LRD-like compact stellar systems with SMBHs.

ACKNOWLEDGMENTS

We are grateful for stimulating discussions with Hou-Zun Chen and Zhaozhou Li. This work was supported by the Israel Science Foundation Grant ISF 861/20, and by the US National Science Foundation - US-Israel Bi-national Science Foundation grants 2023730 and 2023723.

DATA AVAILABILITY

Data and results underlying this article will be shared on reasonable request to the corresponding author.

REFERENCES

- Adamo, A., Bradley, L. D., Vanzella, E., et al. 2024, *Nature*, 632, 513, doi: [10.1038/s41586-024-07703-7](https://doi.org/10.1038/s41586-024-07703-7)
- Akins, H. B., Casey, C. M., Berg, D. A., et al. 2025a, *ApJL*, 980, L29, doi: [10.3847/2041-8213/adab76](https://doi.org/10.3847/2041-8213/adab76)
- Akins, H. B., Casey, C. M., Lambrides, E., et al. 2025b, *ApJ*, 991, 37, doi: [10.3847/1538-4357/ade984](https://doi.org/10.3847/1538-4357/ade984)
- Akins, H. B., Casey, C. M., Chisholm, J., et al. 2025c, arXiv e-prints, arXiv:2503.00998, doi: [10.48550/arXiv.2503.00998](https://doi.org/10.48550/arXiv.2503.00998)
- Andalman, Z. L., Teyssier, R., & Dekel, A. 2025, *MNRAS*, 540, 3350, doi: [10.1093/mnras/staf930](https://doi.org/10.1093/mnras/staf930)
- Baggen, J. F. W., van Dokkum, P., Brammer, G., et al. 2024, *ApJL*, 977, L13, doi: [10.3847/2041-8213/ad90b8](https://doi.org/10.3847/2041-8213/ad90b8)
- Baker, J. G., Centrella, J., Choi, D.-I., Koppitz, M., & van Meter, J. 2006, *PhRvL*, 96, 111102, doi: [10.1103/PhysRevLett.96.111102](https://doi.org/10.1103/PhysRevLett.96.111102)
- Banik, U., & van den Bosch, F. C. 2021, *ApJ*, 912, 43, doi: [10.3847/1538-4357/abeb6d](https://doi.org/10.3847/1538-4357/abeb6d)
- Barro, G., Faber, S. M., Perez-Gonzalez, P. G., et al. 2013, *ApJ*, 765, 104
- Barro, G., Faber, S. M., Koo, D. C., et al. 2017, *ApJ*, 840, 47, doi: [10.3847/1538-4357/aa6b05](https://doi.org/10.3847/1538-4357/aa6b05)
- Barro, G., Pérez-González, P. G., Kocevski, D. D., et al. 2024a, *ApJ*, 963, 128, doi: [10.3847/1538-4357/ad167e](https://doi.org/10.3847/1538-4357/ad167e)
- Barro, G., Perez-Gonzalez, P. G., Kocevski, D. D., et al. 2024b, arXiv e-prints, arXiv:2412.01887, doi: [10.48550/arXiv.2412.01887](https://doi.org/10.48550/arXiv.2412.01887)
- Begelman, M. C., Blandford, R. D., & Rees, M. J. 1980, *Nature*, 287, 307, doi: [10.1038/287307a0](https://doi.org/10.1038/287307a0)
- Billand, J.-B., Elbaz, D., Gentile, F., et al. 2025, arXiv e-prints, arXiv:2507.04011, doi: [10.48550/arXiv.2507.04011](https://doi.org/10.48550/arXiv.2507.04011)
- Binney, J., & Tremaine, S. 2008, *Galactic Dynamics* (Princeton, NJ, Princeton Univ. Press)
- Campanelli, M., Lousto, C. O., Marronetti, P., & Zlochower, Y. 2006, *PhRvL*, 96, 111101, doi: [10.1103/PhysRevLett.96.111101](https://doi.org/10.1103/PhysRevLett.96.111101)
- Casey, C. M., Akins, H. B., Kokorev, V., et al. 2024, *ApJL*, 975, L4, doi: [10.3847/2041-8213/ad7ba7](https://doi.org/10.3847/2041-8213/ad7ba7)
- Casey, C. M., Akins, H. B., Finkelstein, S. L., et al. 2025, *ApJL*, 990, L61, doi: [10.3847/2041-8213/adfa91](https://doi.org/10.3847/2041-8213/adfa91)
- Cataldi, P., Pedrosa, S., Pellizza, L. J., Ceverino, D., & Bignone, L. A. 2025, arXiv e-prints, arXiv:2510.05299, doi: [10.48550/arXiv.2510.05299](https://doi.org/10.48550/arXiv.2510.05299)
- Ceverino, D., Dekel, A., Mandelker, N., et al. 2012, *MNRAS*, 420, 3490, doi: [10.1111/j.1365-2966.2011.20296.x](https://doi.org/10.1111/j.1365-2966.2011.20296.x)
- Ceverino, D., & Klypin, A. 2009, *ApJ*, 695, 292
- Ceverino, D., Klypin, A., Klimek, E. S., et al. 2014, *MNRAS*, 442, 1545
- Ceverino, D., Primack, J., Dekel, A., & Kasin, S. A. 2017, *MNRAS*, 467, 2664, doi: [10.1093/mnras/stx289](https://doi.org/10.1093/mnras/stx289)
- Chandrasekhar, S. 1943, *ApJ*, 97, 255, doi: [10.1086/144517](https://doi.org/10.1086/144517)
- Claeysens, A., Adamo, A., Richard, J., et al. 2023, *MNRAS*, 520, 2180, doi: [10.1093/mnras/stac3791](https://doi.org/10.1093/mnras/stac3791)
- Cole, S., Lacey, C. G., Baugh, C. M., & Frenk, C. S. 2000, *MNRAS*, 319, 168, doi: [10.1046/j.1365-8711.2000.03879.x](https://doi.org/10.1046/j.1365-8711.2000.03879.x)
- Covington, M., Dekel, A., Cox, T. J., Jonsson, P., & Primack, J. R. 2008, *MNRAS*, 384, 94
- de Graaff, A., Setton, D. J., Brammer, G., et al. 2024, *Nature Astronomy*, doi: [10.1038/s41550-024-02424-3](https://doi.org/10.1038/s41550-024-02424-3)
- Dekel, A., & Burkert, A. 2014, *MNRAS*, 438, 1870
- Dekel, A., Ginzburg, O., Jiang, F., et al. 2020a, *MNRAS*, 493, 4126, doi: [10.1093/mnras/staa470](https://doi.org/10.1093/mnras/staa470)
- Dekel, A., Lapiner, S., & Dubois, Y. 2019, arXiv e-prints, arXiv:1904.08431, doi: [10.48550/arXiv.1904.08431](https://doi.org/10.48550/arXiv.1904.08431)
- Dekel, A., Lecar, M., & Shaham, J. 1980, *ApJ*, 241, 946, doi: [10.1086/158409](https://doi.org/10.1086/158409)
- Dekel, A., Mandelker, N., Li, Z., et al. 2025a, arXiv e-prints, arXiv:2506.11664, doi: [10.48550/arXiv.2506.11664](https://doi.org/10.48550/arXiv.2506.11664)
- Dekel, A., Sarkar, K. C., Birnboim, Y., Mandelker, N., & Li, Z. 2023, *MNRAS*, 523, 3201, doi: [10.1093/mnras/stad1557](https://doi.org/10.1093/mnras/stad1557)
- Dekel, A., Stone, N. C., Chowdhury, D. D., et al. 2025b, *A&A*, 695, A97, doi: [10.1051/0004-6361/202452393](https://doi.org/10.1051/0004-6361/202452393)
- Dekel, A., Lapiner, S., Ginzburg, O., et al. 2020b, *MNRAS*, 496, 5372, doi: [10.1093/mnras/staa1713](https://doi.org/10.1093/mnras/staa1713)

- Dekel, A., Freundlich, J., Jiang, F., et al. 2021, arXiv e-prints, arXiv:2106.01378
- Devecchi, B., & Volonteri, M. 2009, ApJ, 694, 302, doi: [10.1088/0004-637X/694/1/302](https://doi.org/10.1088/0004-637X/694/1/302)
- Dubois, Y., Pichon, C., Haehnelt, M., et al. 2012, MNRAS, 423, 3616, doi: [10.1111/j.1365-2966.2012.21160.x](https://doi.org/10.1111/j.1365-2966.2012.21160.x)
- Dubois, Y., Beckmann, R., Bournaud, F., et al. 2021, A&A, 651, A109, doi: [10.1051/0004-6361/202039429](https://doi.org/10.1051/0004-6361/202039429)
- Dutta Chowdhury, D., Dekel, A., Mandelker, N., Ginzburg, O., & Genzel, R. 2024, arXiv e-prints, arXiv:2409.01589, doi: [10.48550/arXiv.2409.01589](https://doi.org/10.48550/arXiv.2409.01589)
- Ernst, A., Glaschke, P., Fiestas, J., Just, A., & Spurzem, R. 2007, MNRAS, 377, 465, doi: [10.1111/j.1365-2966.2007.11602.x](https://doi.org/10.1111/j.1365-2966.2007.11602.x)
- Fujimoto, S., Arrabal Haro, P., Dickinson, M., et al. 2023, arXiv e-prints, arXiv:2301.09482, doi: [10.48550/arXiv.2301.09482](https://doi.org/10.48550/arXiv.2301.09482)
- Giersz, M., & Heggie, D. C. 1994, MNRAS, 268, 257, doi: [10.1093/mnras/268.1.257](https://doi.org/10.1093/mnras/268.1.257)
- GoerdT, T., Moore, B., Read, J. I., Stadel, J., & Zemp, M. 2006, MNRAS, 368, 1073, doi: [10.1111/j.1365-2966.2006.10182.x](https://doi.org/10.1111/j.1365-2966.2006.10182.x)
- Greene, J. E., Labbe, I., Goulding, A. D., et al. 2024, ApJ, 964, 39, doi: [10.3847/1538-4357/ad1e5f](https://doi.org/10.3847/1538-4357/ad1e5f)
- Greene, J. E., Setton, D. J., Furtak, L. J., et al. 2025, arXiv e-prints, arXiv:2509.05434, doi: [10.48550/arXiv.2509.05434](https://doi.org/10.48550/arXiv.2509.05434)
- Gronke, M., Oh, S. P., Ji, S., & Norman, C. 2022, MNRAS, 511, 859, doi: [10.1093/mnras/stab3351](https://doi.org/10.1093/mnras/stab3351)
- Hachisu, I. 1979, PASJ, 31, 523
- Hachisu, I. 1982, PASJ, 34, 313
- Hatton, S., Devriendt, J. E. G., Ninin, S., et al. 2003, MNRAS, 343, 75
- Hong, J., Kim, E., Lee, H. M., & Spurzem, R. 2013, MNRAS, 430, 2960, doi: [10.1093/mnras/stt099](https://doi.org/10.1093/mnras/stt099)
- Hopkins, P. F. 2015, MNRAS, 450, 53, doi: [10.1093/mnras/stv195](https://doi.org/10.1093/mnras/stv195)
- Hopkins, P. F., Cox, T. J., Hernquist, L., et al. 2013, MNRAS, 430, 1901, doi: [10.1093/mnras/stt017](https://doi.org/10.1093/mnras/stt017)
- Huertas-Company, M., Primack, J. R., Dekel, A., et al. 2018, ApJ, 858, 114, doi: [10.3847/1538-4357/aabfed](https://doi.org/10.3847/1538-4357/aabfed)
- Jones, B. L., Kocevski, D. D., Pacucci, F., et al. 2025, arXiv e-prints, arXiv:2510.07376, doi: [10.48550/arXiv.2510.07376](https://doi.org/10.48550/arXiv.2510.07376)
- Kamlah, A. W. H., Spurzem, R., Berczik, P., et al. 2022, MNRAS, 516, 3266, doi: [10.1093/mnras/stac2281](https://doi.org/10.1093/mnras/stac2281)
- Katz, H., Sijacki, D., & Haehnelt, M. G. 2015, MNRAS, 451, 2352, doi: [10.1093/mnras/stv1048](https://doi.org/10.1093/mnras/stv1048)
- Kaur, K., & Sridhar, S. 2018, ApJ, 868, 134, doi: [10.3847/1538-4357/aaeacf](https://doi.org/10.3847/1538-4357/aaeacf)
- Kim, E., Yoon, I., Lee, H. M., & Spurzem, R. 2008, MNRAS, 383, 2, doi: [10.1111/j.1365-2966.2007.12524.x](https://doi.org/10.1111/j.1365-2966.2007.12524.x)
- Kocevski, D. D., Finkelstein, S. L., Barro, G., et al. 2025, ApJ, 986, 126, doi: [10.3847/1538-4357/adbc7d](https://doi.org/10.3847/1538-4357/adbc7d)
- Kokorev, V., Caputi, K. I., Greene, J. E., et al. 2024, ApJ, 968, 38, doi: [10.3847/1538-4357/ad4265](https://doi.org/10.3847/1538-4357/ad4265)
- Kravtsov, A. V., Klypin, A. A., & Khokhlov, A. M. 1997, ApJS, 111, 73
- Kroupa, P. 2001, MNRAS, 322, 231, doi: [10.1046/j.1365-8711.2001.04022.x](https://doi.org/10.1046/j.1365-8711.2001.04022.x)
- Lapiner, S., Dekel, A., & Dubois, Y. 2021, MNRAS, 505, 172, doi: [10.1093/mnras/stab1205](https://doi.org/10.1093/mnras/stab1205)
- Lapiner, S., Dekel, A., Freundlich, J., et al. 2023, MNRAS, 522, 4515, doi: [10.1093/mnras/stad1263](https://doi.org/10.1093/mnras/stad1263)
- Li, Z., Dekel, A., Sarkar, K. C., et al. 2024, A&A, 690, A108, doi: [10.1051/0004-6361/202348727](https://doi.org/10.1051/0004-6361/202348727)
- Lynden-Bell, D., & Wood, R. 1968, MNRAS, 138, 495, doi: [10.1093/mnras/138.4.495](https://doi.org/10.1093/mnras/138.4.495)
- Mandelker, N., Dekel, A., Ceverino, D., et al. 2017, MNRAS, 464, 635, doi: [10.1093/mnras/stw2358](https://doi.org/10.1093/mnras/stw2358)
- Mandelker, N., Dekel, A., Ceverino, D., et al. 2014, MNRAS, 443, 3675
- Martig, M., Bournaud, F., Teyssier, R., & Dekel, A. 2009, ApJ, 707, 250
- Mayer, L., & Bonoli, S. 2019, Reports on Progress in Physics, 82, 016901, doi: [10.1088/1361-6633/aad6a5](https://doi.org/10.1088/1361-6633/aad6a5)
- Mayer, L., Capelo, P. R., Zwick, L., & Di Matteo, T. 2024, ApJ, 961, 76, doi: [10.3847/1538-4357/ad11cf](https://doi.org/10.3847/1538-4357/ad11cf)
- Mayer, L., Fiacconi, D., Bonoli, S., et al. 2015, ApJ, 810, 51, doi: [10.1088/0004-637X/810/1/51](https://doi.org/10.1088/0004-637X/810/1/51)
- Messa, M., Dessauges-Zavadsky, M., Adamo, A., Richard, J., & Claeysens, A. 2024, MNRAS, 529, 2162, doi: [10.1093/mnras/stae565](https://doi.org/10.1093/mnras/stae565)
- Mowla, L. 2024, Nature, 632, 505, doi: [10.1038/d41586-024-02438-x](https://doi.org/10.1038/d41586-024-02438-x)
- Mowla, L., Iyer, K., Asada, Y., et al. 2024, Nature, 636, 332, doi: [10.1038/s41586-024-08293-0](https://doi.org/10.1038/s41586-024-08293-0)
- Pacucci, F. 2024, Scientific American, 331, E1
- Pacucci, F., Hernquist, L., & Fujii, M. 2025, arXiv e-prints, arXiv:2509.02664, doi: [10.48550/arXiv.2509.02664](https://doi.org/10.48550/arXiv.2509.02664)
- Pacucci, F., & Loeb, A. 2025, ApJL, 989, L19, doi: [10.3847/2041-8213/ade871](https://doi.org/10.3847/2041-8213/ade871)
- Pacucci, F., & Narayan, R. 2024, ApJ, 976, 96, doi: [10.3847/1538-4357/ad84f7](https://doi.org/10.3847/1538-4357/ad84f7)
- Portegies Zwart, S. F., Baumgardt, H., Hut, P., Makino, J., & McMillan, S. L. W. 2004, Nature, 428, 724, doi: [10.1038/nature02448](https://doi.org/10.1038/nature02448)
- Portegies Zwart, S. F., & McMillan, S. L. W. 2002, ApJ, 576, 899, doi: [10.1086/341798](https://doi.org/10.1086/341798)
- Pretorius, F. 2005, PhRvL, 95, 121101, doi: [10.1103/PhysRevLett.95.121101](https://doi.org/10.1103/PhysRevLett.95.121101)
- Rantala, A., Naab, T., & Lahén, N. 2024, arXiv e-prints, arXiv:2403.10602, doi: [10.48550/arXiv.2403.10602](https://doi.org/10.48550/arXiv.2403.10602)

- Read, J. I., Goerdt, T., Moore, B., et al. 2006, MNRAS, 373, 1451, doi: [10.1111/j.1365-2966.2006.11022.x](https://doi.org/10.1111/j.1365-2966.2006.11022.x)
- Rizzuto, F. P., Naab, T., Spurzem, R. e., et al. 2021, MNRAS, 501, 5257, doi: [10.1093/mnras/staa3634](https://doi.org/10.1093/mnras/staa3634)
- Saijo, M., & Hawke, I. 2009, PhRvD, 80, 064001, doi: [10.1103/PhysRevD.80.064001](https://doi.org/10.1103/PhysRevD.80.064001)
- Shen, S., Mo, H. J., White, S. D. M., et al. 2003, MNRAS, 343, 978
- Shibata, M., & Shapiro, S. L. 2002, ApJL, 572, L39, doi: [10.1086/341516](https://doi.org/10.1086/341516)
- Spitzer, Lyman, J., & Hart, M. H. 1971, ApJ, 164, 399, doi: [10.1086/150855](https://doi.org/10.1086/150855)
- Spitzer, Jr., L. 1958, ApJ, 127, 17, doi: [10.1086/146435](https://doi.org/10.1086/146435)
- Tacchella, S., Dekel, A., Carollo, C. M., et al. 2016a, MNRAS, 458, 242, doi: [10.1093/mnras/stw303](https://doi.org/10.1093/mnras/stw303)
- Tacchella, S., Dekel, A., Carollo, C. M., et al. 2016b, MNRAS, 457, 2790, doi: [10.1093/mnras/stw131](https://doi.org/10.1093/mnras/stw131)
- Taylor, A. J., Akins, H., Finkelstein, S. L., et al. 2025a, Balmer Breaks in Little Red Dots: Stellar Populations or Dense Neutral Gas?, JWST Proposal. Cycle 4, ID. #8520
- Taylor, A. J., Finkelstein, S. L., Kocevski, D. D., et al. 2025b, ApJ, 986, 165, doi: [10.3847/1538-4357/add15b](https://doi.org/10.3847/1538-4357/add15b)
- Teyssier, R. 2002, A&A, 385, 337
- Tomassetti, M., Dekel, A., Mandelker, N., et al. 2016, MNRAS, 458, 4477, doi: [10.1093/mnras/stw606](https://doi.org/10.1093/mnras/stw606)
- Tremaine, S., & Weinberg, M. D. 1984, MNRAS, 209, 729, doi: [10.1093/mnras/209.4.729](https://doi.org/10.1093/mnras/209.4.729)
- Trujillo-Gomez, S., Reina-Campos, M., & Kruijssen, J. M. D. 2019, MNRAS, 488, 3972, doi: [10.1093/mnras/stz1932](https://doi.org/10.1093/mnras/stz1932)
- van Dokkum, P. G., Nelson, E. J., Franx, M., et al. 2015, ApJ, 813, 23, doi: [10.1088/0004-637X/813/1/23](https://doi.org/10.1088/0004-637X/813/1/23)
- Vanzella, E., Claeysens, A., Welch, B., et al. 2023, ApJ, 945, 53, doi: [10.3847/1538-4357/acb59a](https://doi.org/10.3847/1538-4357/acb59a)
- Vergara, M. C., Askar, A., Flammini Dotti, F., et al. 2025a, arXiv e-prints, arXiv:2508.14260, doi: [10.48550/arXiv.2508.14260](https://doi.org/10.48550/arXiv.2508.14260)
- Vergara, M. C., Askar, A., Kamlah, A. W. H., et al. 2025b, arXiv e-prints, arXiv:2505.07491, doi: [10.48550/arXiv.2505.07491](https://doi.org/10.48550/arXiv.2505.07491)
- Wadsley, J. W., Keller, B. W., & Quinn, T. R. 2017, MNRAS, 471, 2357, doi: [10.1093/mnras/stx1643](https://doi.org/10.1093/mnras/stx1643)
- Zolotov, A., Dekel, A., Mandelker, N., et al. 2015, MNRAS, 450, 2327, doi: [10.1093/mnras/stv740](https://doi.org/10.1093/mnras/stv740)
- Zwick, L., Mayer, L., Haemmerlé, L., & Klessen, R. S. 2023, MNRAS, 518, 2076, doi: [10.1093/mnras/stac3204](https://doi.org/10.1093/mnras/stac3204)
- Zwick, L., Tiede, C., & Mayer, L. 2025, arXiv e-prints, arXiv:2507.22014, doi: [10.48550/arXiv.2507.22014](https://doi.org/10.48550/arXiv.2507.22014)